Blessed Plots for the Forward Horn Current 7.1×10^{20} POT Antineutrino Analysis

J. Evans, J. Hartnell, D. Naples, B. Pahlka, R. Sharma, M. Mathis, P. Vahle and Z. Isvan
for the NuMuBar Group

April 28, 2011
Version 16
(minos-doc-7906-v16)

Brief Overview

This document contains the blessed plots for the analysis of the 7% $\overline{\nu}_\mu$ component in the FHC (ν_μ-mode) NuMI beam. The analysis uses the runs 1–3 LE data, corresponding to an exposure of 7.1×10^{20} protons on target.

The goal of this analysis is to determine the spectrum of $\overline{\nu}_\mu$ events in the Far Detector in order to extract physics model parameters. The search for $\overline{\nu}_\mu$ disappearance constrains $\overline{\nu}_\mu \rightarrow \overline{\nu}_\tau$ oscillation parameters. In particular, $\overline{\nu}_\mu$ disappearance will constrain oscillation parameters $\Delta\overline{m}^2$ and $\sin^2(2\overline{\theta}_{23})$ through the measured oscillation probability,

$$P(\overline{\nu}_\mu \rightarrow \overline{\nu}_\mu) = 1 - \sin^2(2\overline{\theta}_{23}) \sin^2(1.267\Delta\overline{m}^2 \frac{L}{E}).$$

Selection Efficiency and Purity

minos-doc-5415

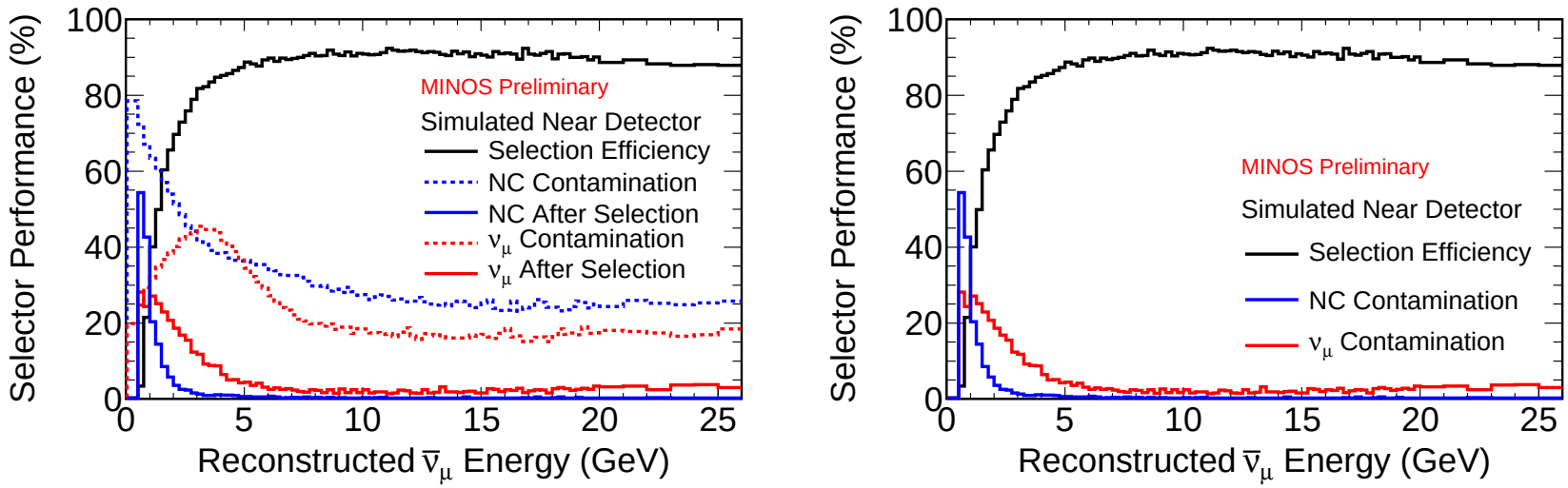

Figure 1: Performance of the current FHC 'Bravo' selector (David Petyt's PID > 0.25, $\sigma(qp)/(qp) > 3.5$, $|\text{relative angle} - \pi| > 2.12$) in the Near Detector. The dashed lines show the contamination before selection and the solid show efficiency and contamination after selection. The ν_μ contamination rises at higher energies since these tracks do not curve as much and so are more difficult to assign a charge to.

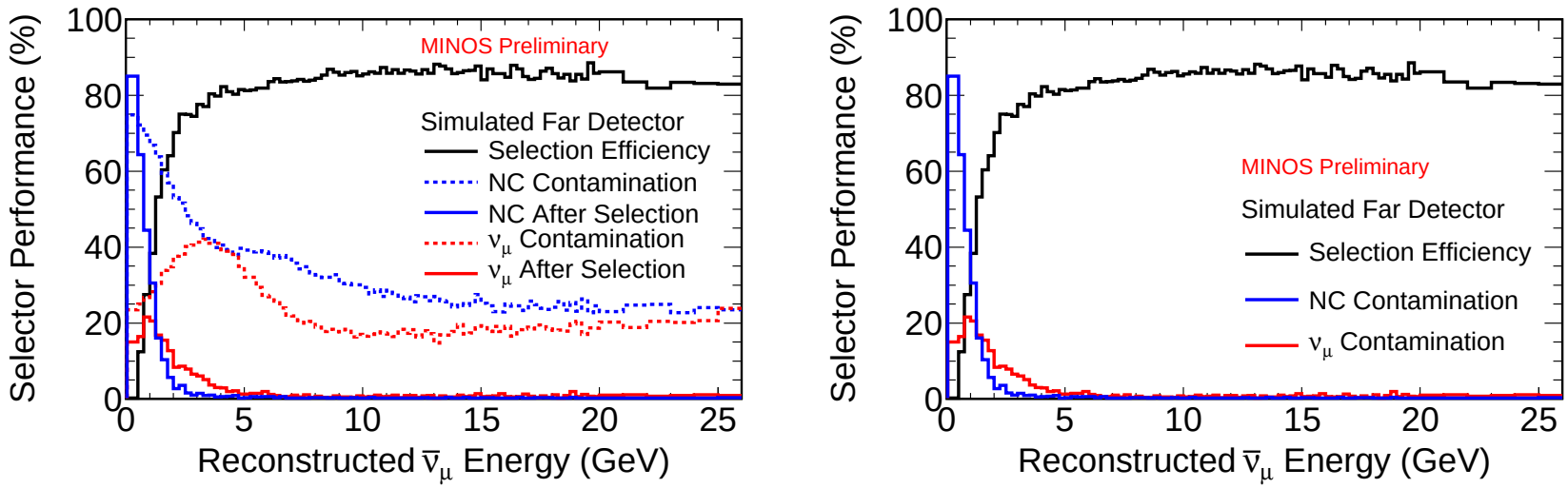

Figure 2: Performance of the current FHC 'Bravo' selector (David Petyt's PID > 0.25, $\sigma(qp)/(qp) > 3.5$, $|\text{relative angle} - \pi| > 2.12$) in the Far Detector. The dashed lines show the contamination before selection and the solid show efficiency and contamination after selection. The ν_μ contamination rises at higher energies since these tracks do not curve as much and so are more difficult to assign a charge to.

ND Data/MC distributions

minos-doc-7767 minos-doc-7873

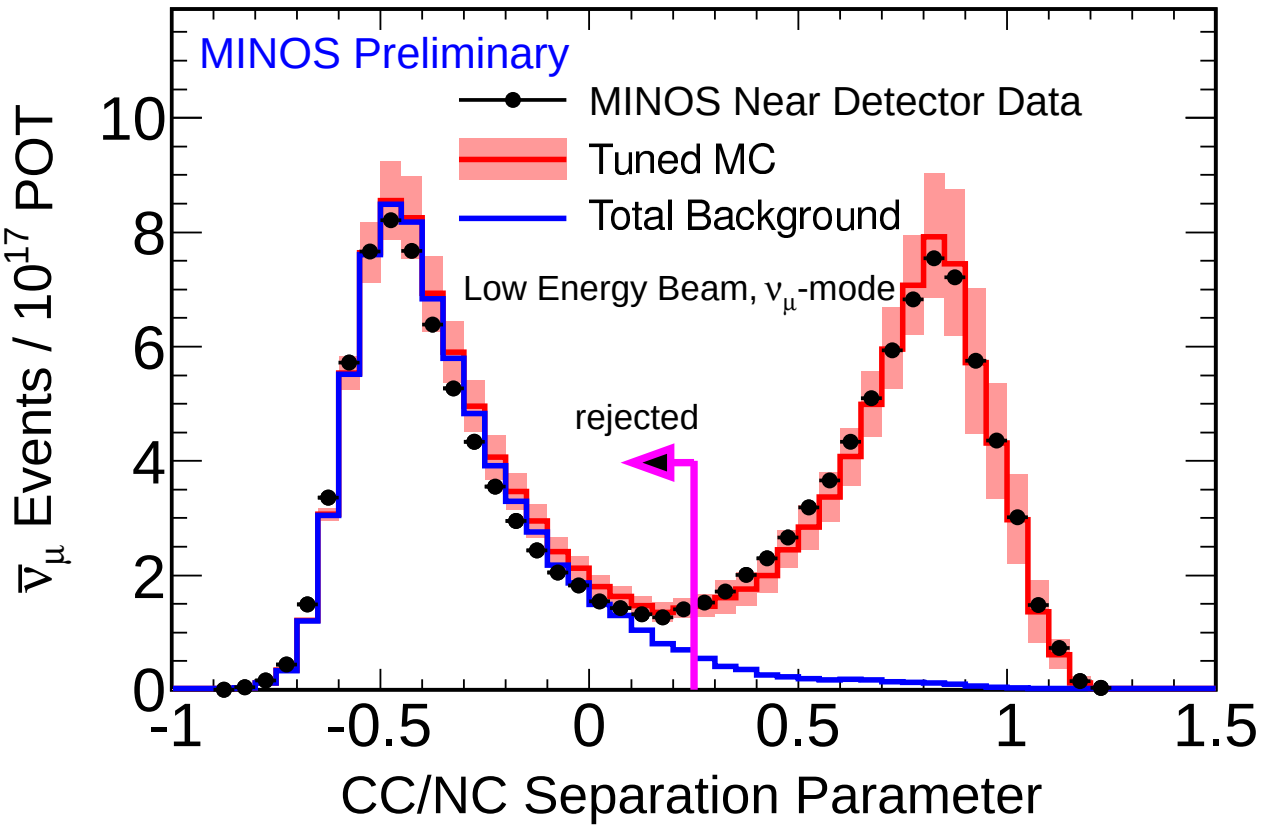

Figure 3: CC/NC separation parameter of events passing all other selection cuts. The red histogram represents the Monte Carlo expectation with the systematic error, the blue histogram represents the total (charged and neutral current) background. Black points represent data. The cut removes events with PID< 0.25

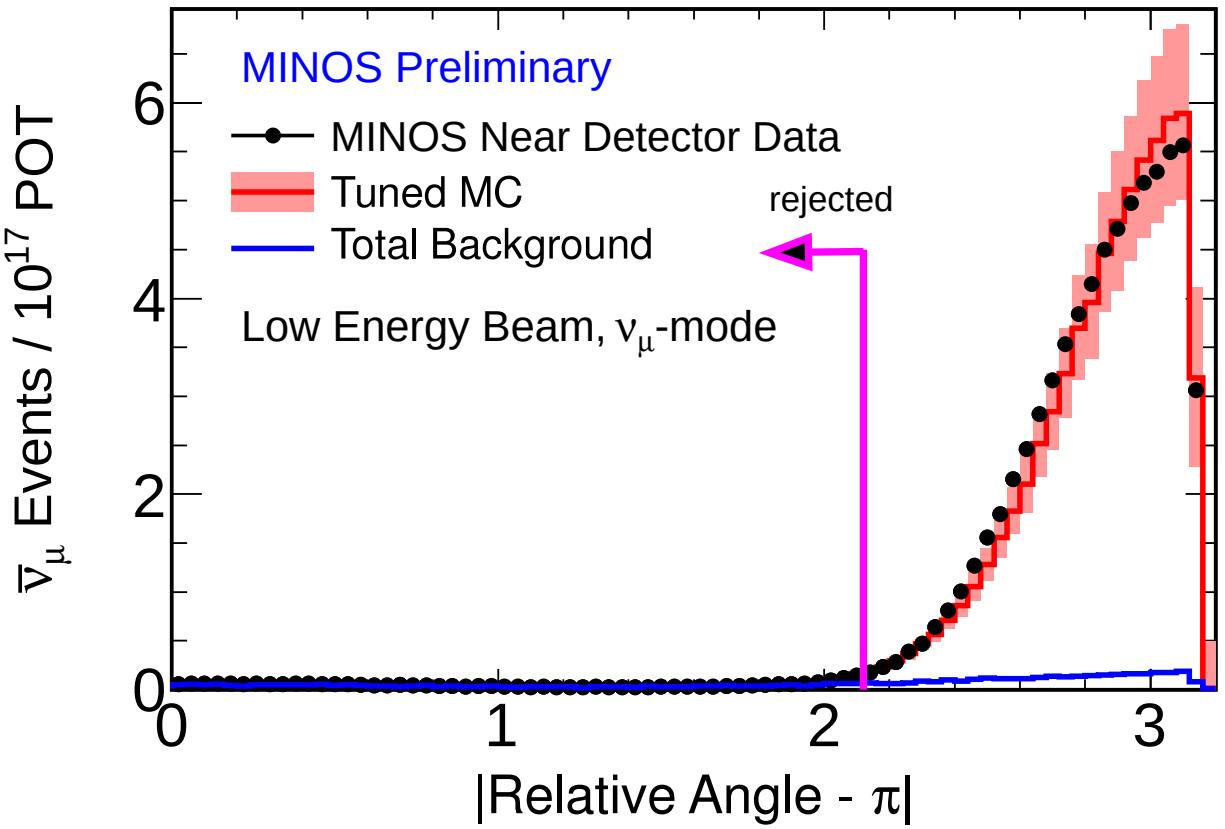

Figure 4: Near Detector *relative angle* distribution of events passing all other selection cuts. The red histogram represents the Monte Carlo expectation with the systematic error, the blue histogram represents the total (charged and neutral current) background. Black points represent data. The cut removes events with $|\text{relative angle} - \pi| < 2.12$.

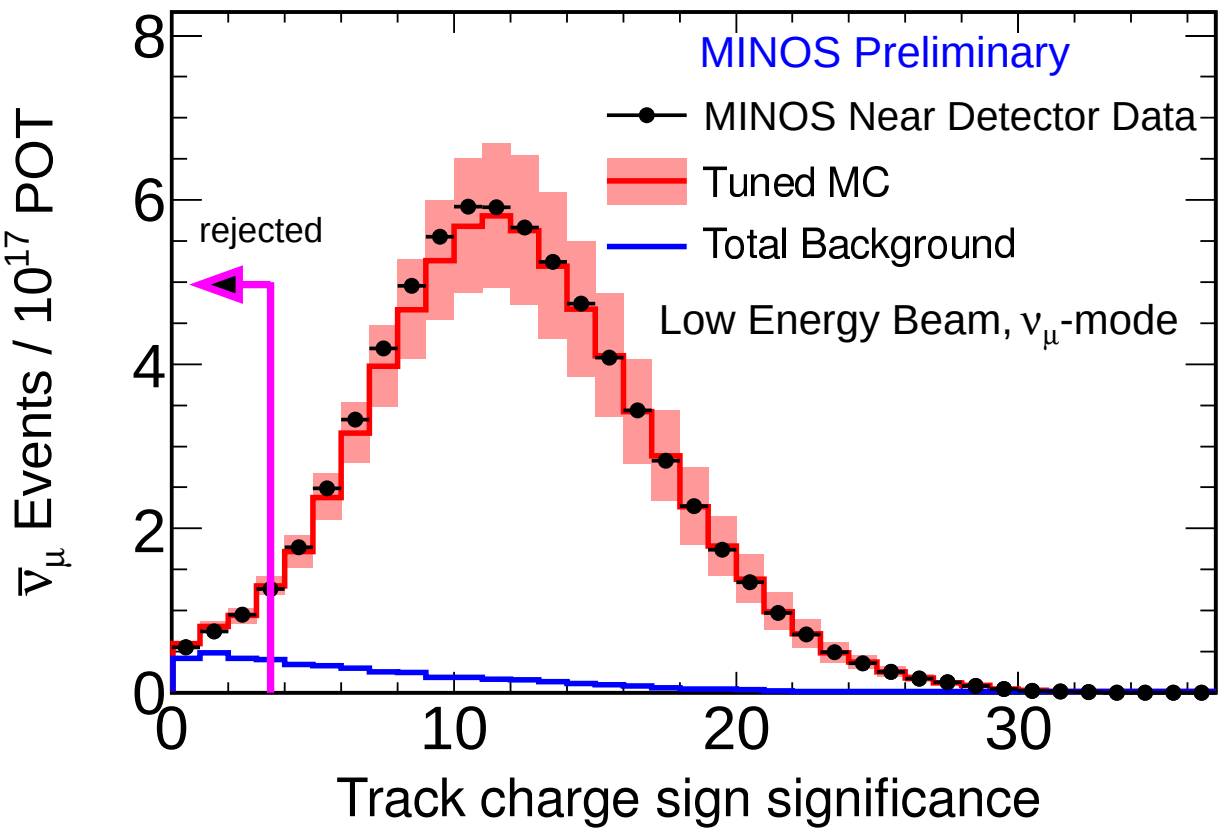

Figure 5: $(q/p)/\sigma(q/p)$ *track charge sign significance* distribution of events passing all other selection cuts in the Near Detector. The red curve represents MC expectation with the systematic uncertainty, the blue curve represents the CC and NC backgrounds and black dots represent data.

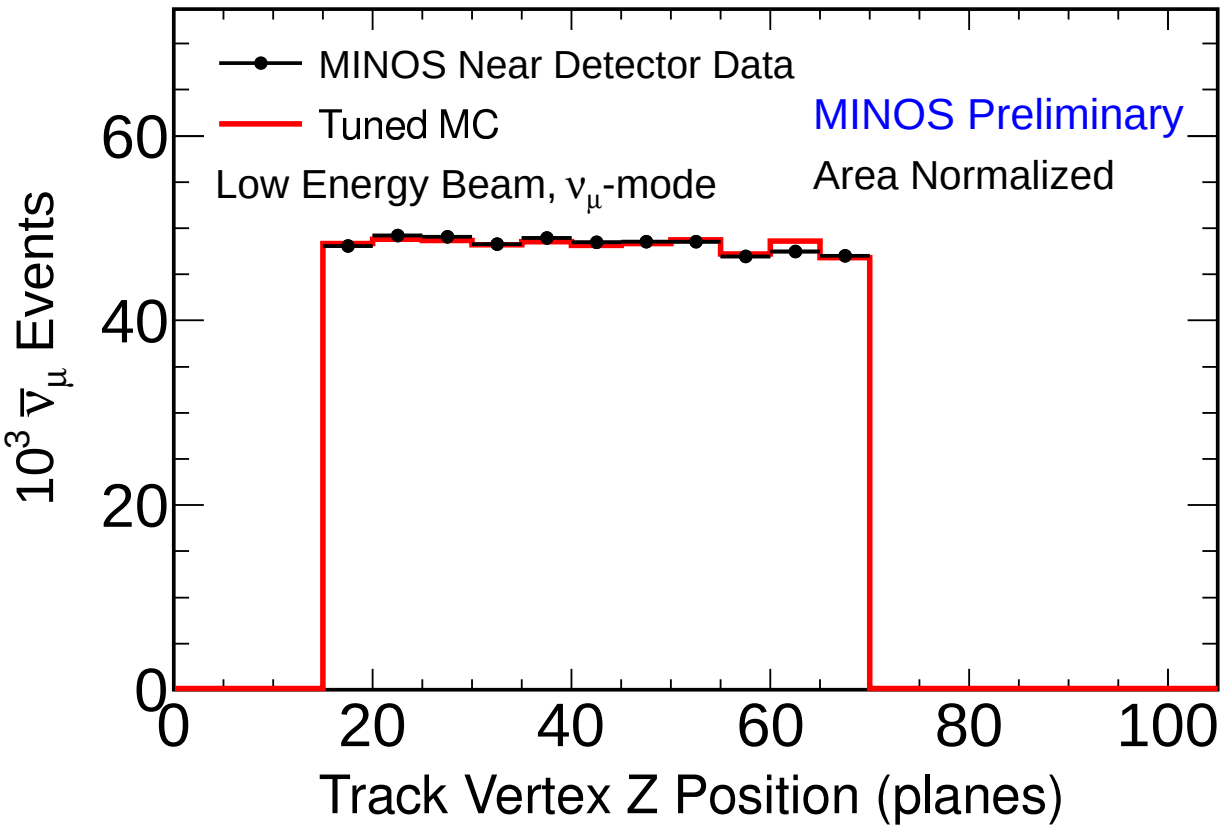

Figure 6: Near Detector track vertex longitudinal position distribution in planes. The red histogram represents the Monte Carlo expectation and black points represent data.

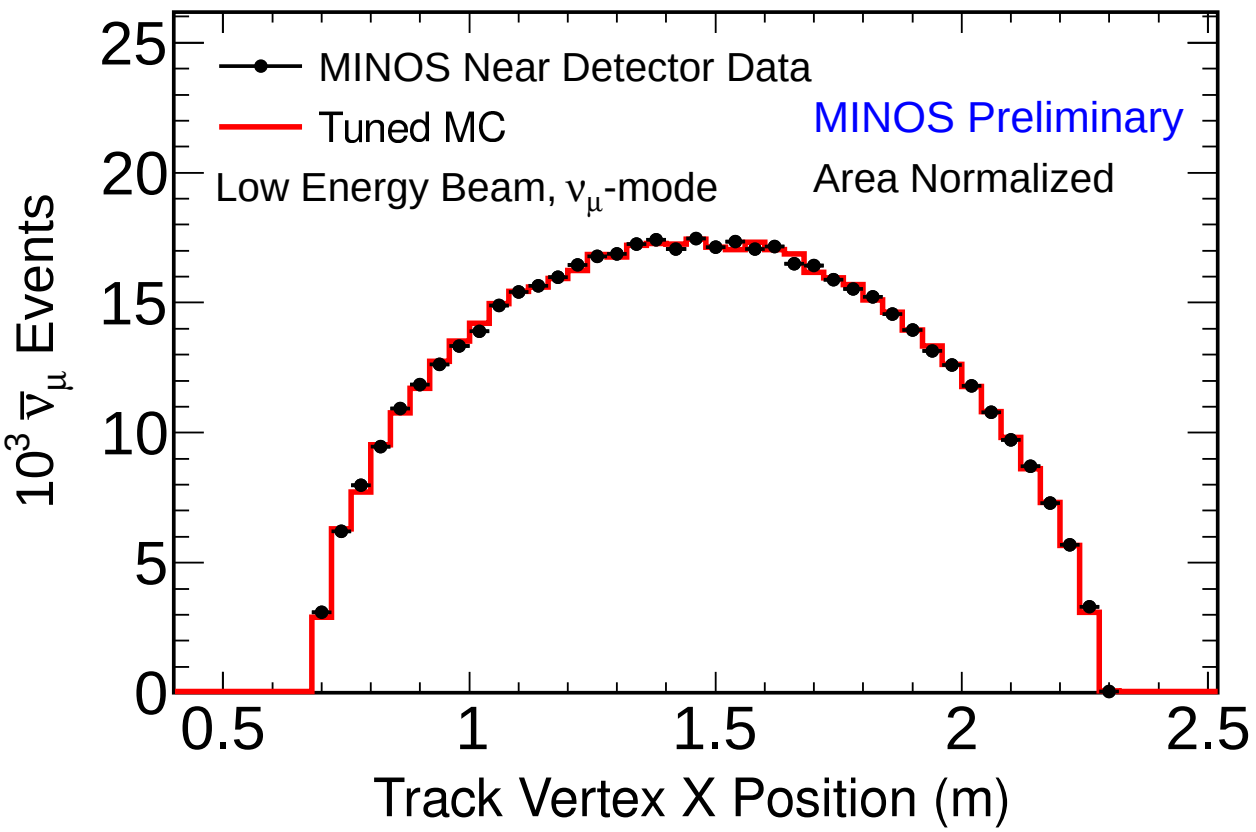

Figure 7: Near Detector track vertex X position distribution. The red histogram represents the Monte Carlo expectation and black points represent data.

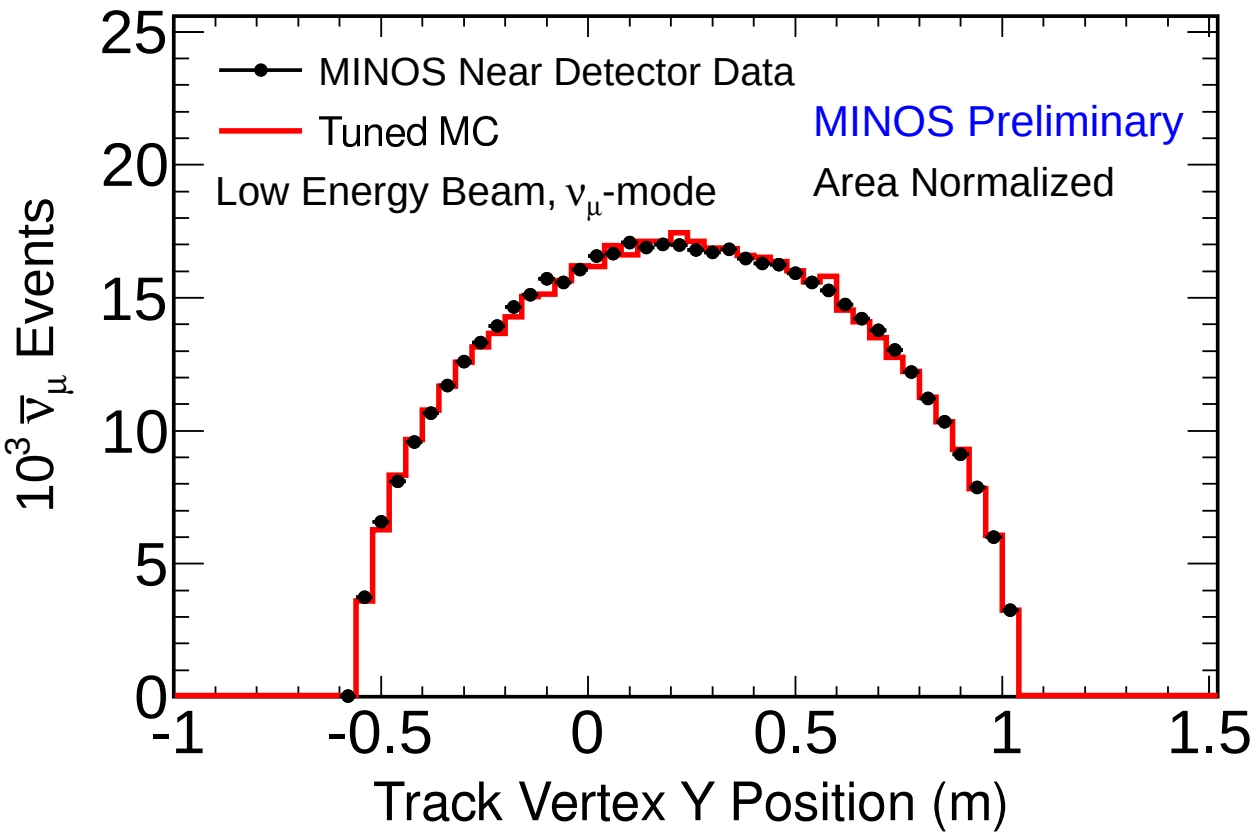

Figure 8: Near Detector track vertex Y position distribution. The red histogram represents the Monte Carlo expectation and black points represent data.

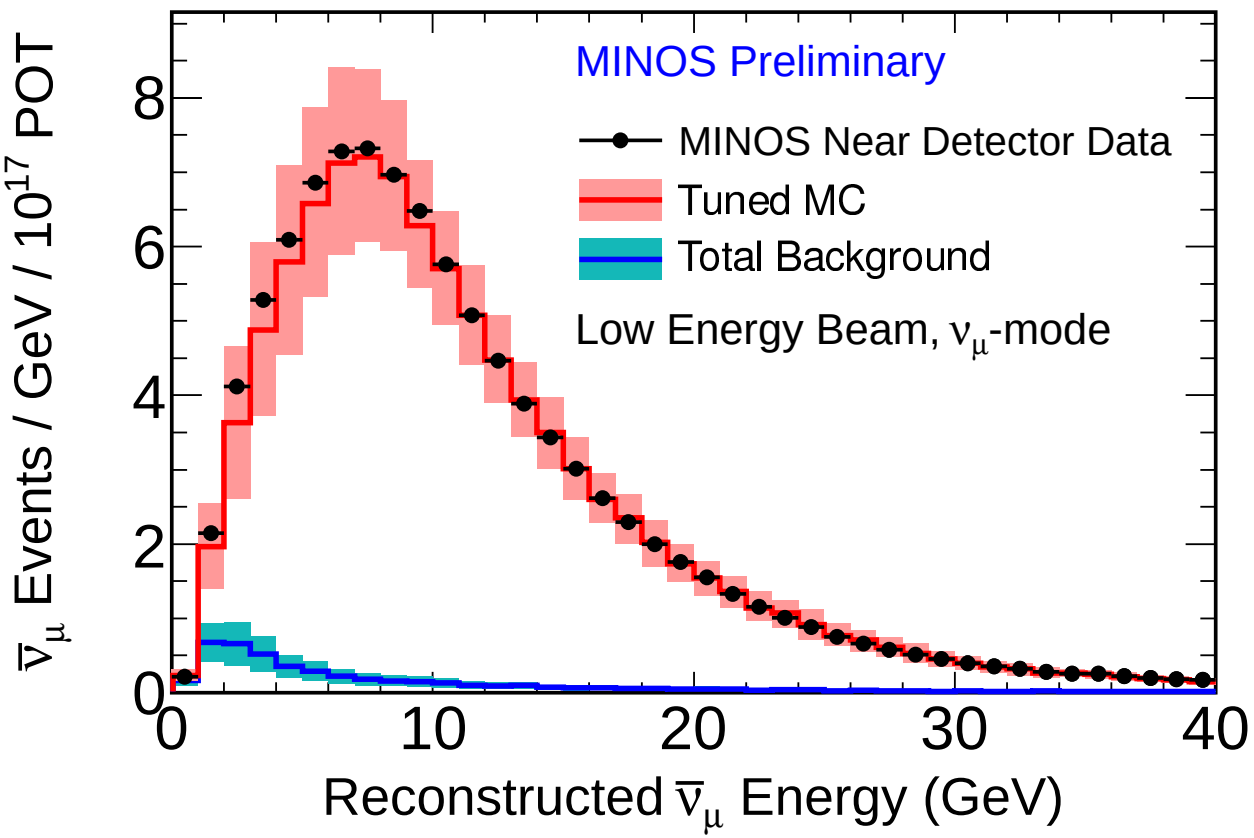

Figure 9: Reconstructed energy distribution of events selected as antineutrinos in the Near Detector. The red histogram represents the Monte Carlo expectation with the systematic error, the blue histogram represents the total (charged and neutral current) background with the background uncertainty. Black points represent data.

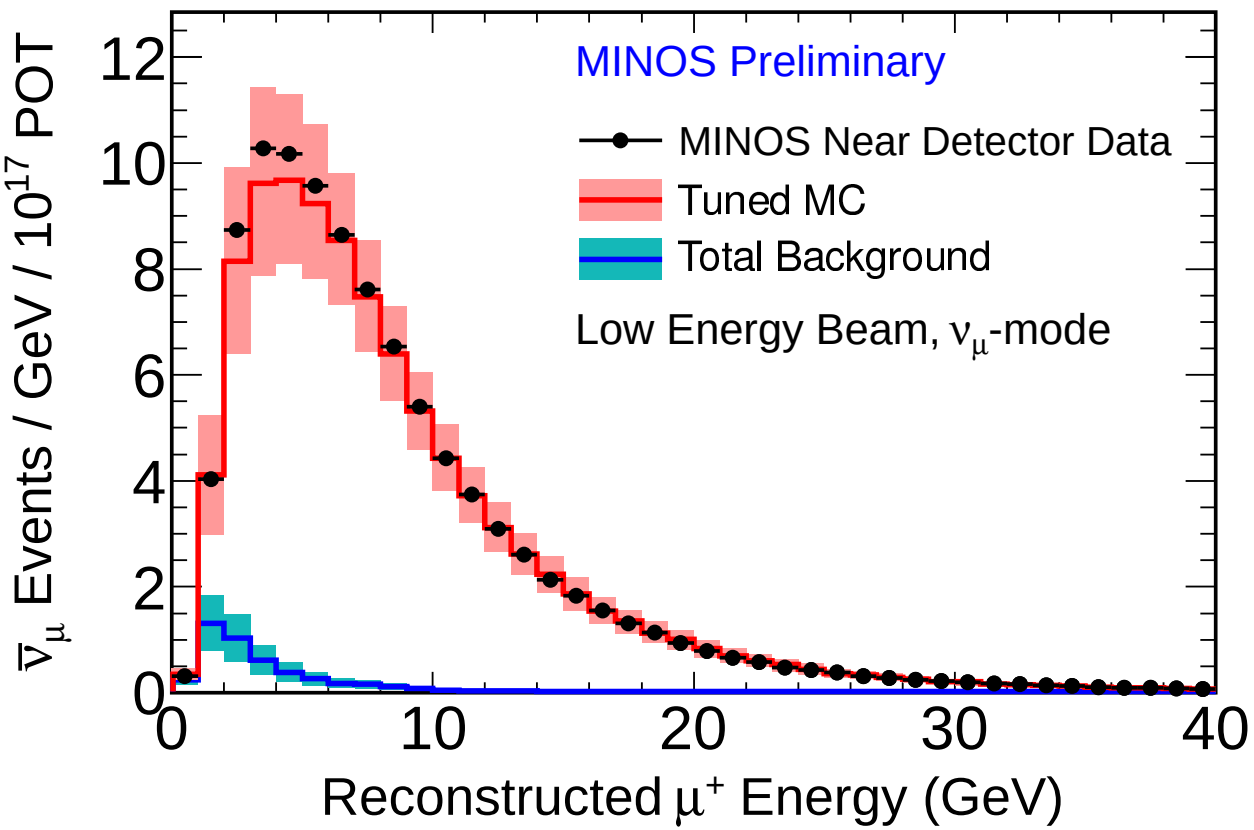

Figure 10: Reconstructed momentum of μ^+ tracks in the Near Detector. The red histogram represents the Monte Carlo expectation with the systematic error, the blue histogram represents the total (charged and neutral current) background with the background uncertainty. Black points represent data.

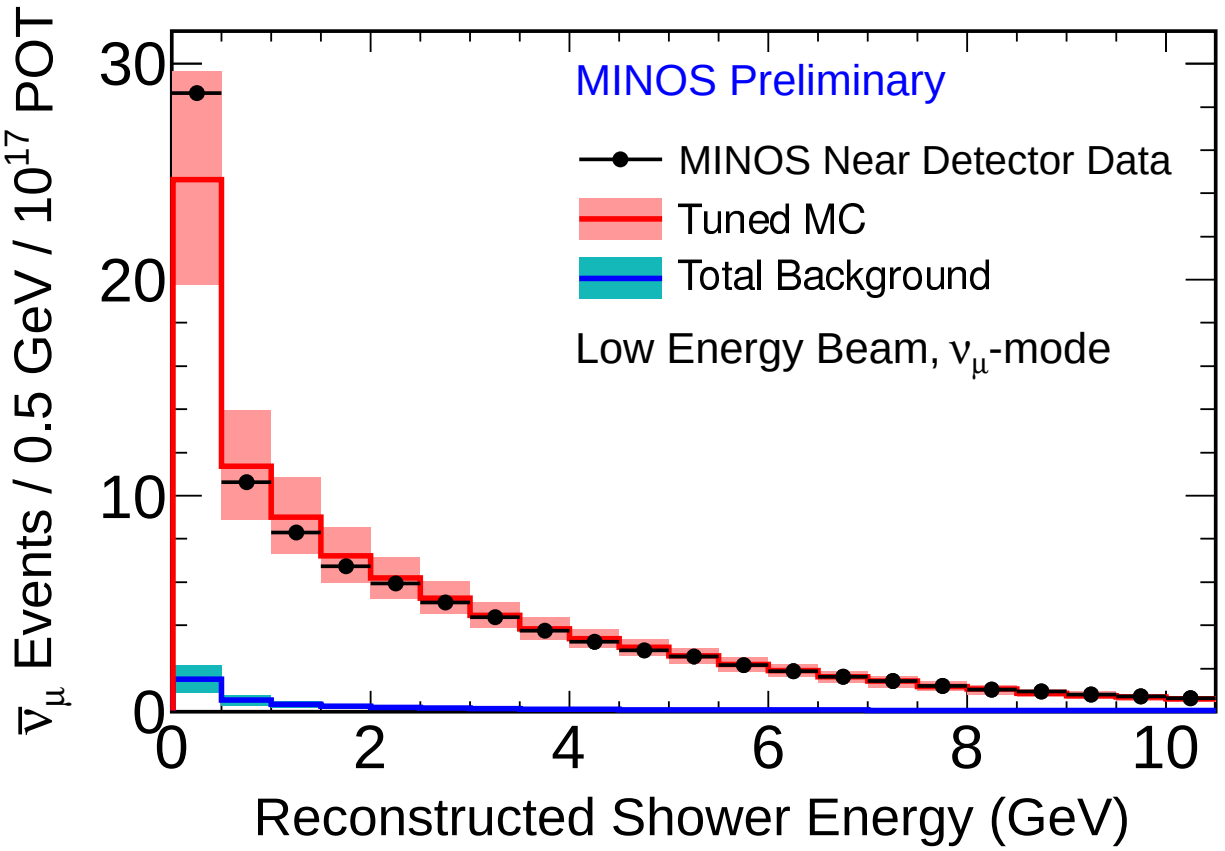

Figure 11: Reconstructed (calorimetric) shower energy distribution in the Near Detector. The red histogram represents the Monte Carlo expectation with the systematic error, the blue histogram represents the total (charged and neutral current) background with the background uncertainty. Black points represent data.

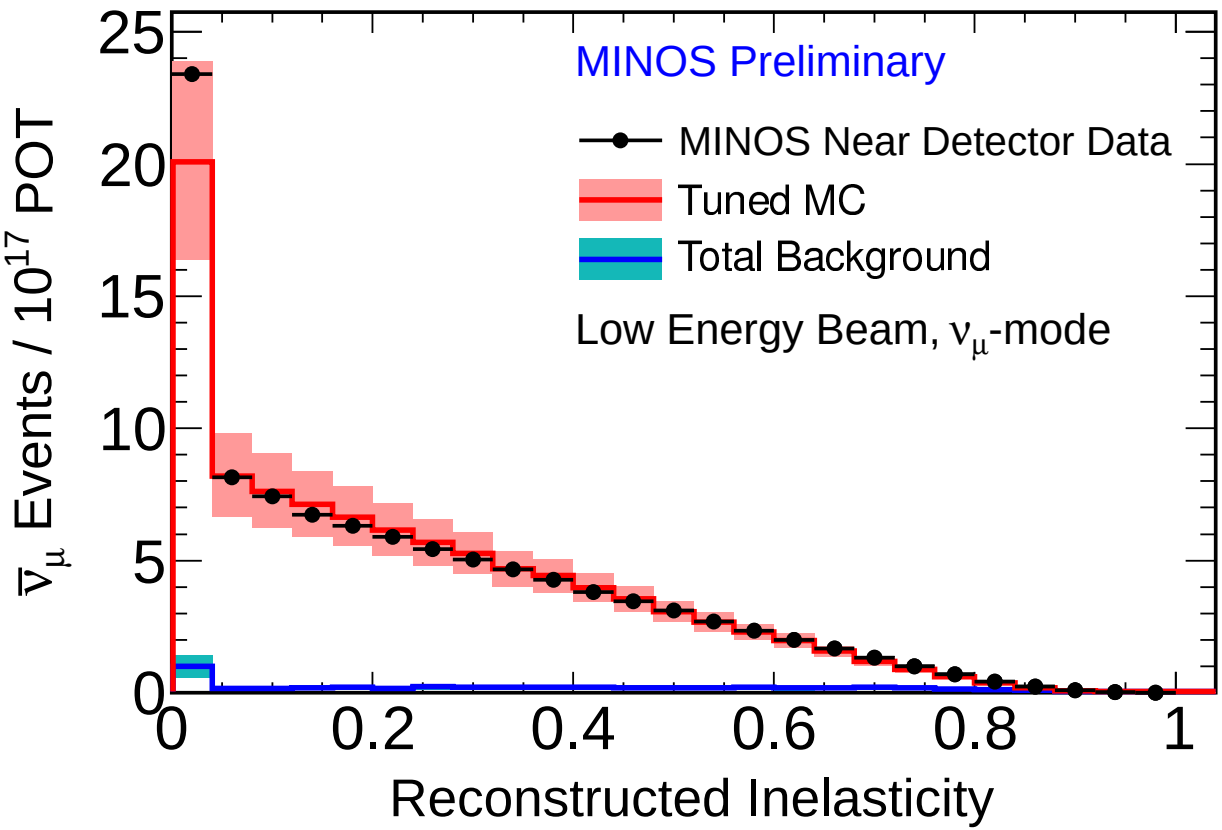

Figure 12: Reconstructed inelasticity distribution in the Near Detector. The red histogram represents the Monte Carlo expectation with the systematic error, the blue histogram represents the total (charged and neutral current) background with the background uncertainty. Black points represent data.

FD Data/MC distributions

minos-doc-7824 minos-doc-7859

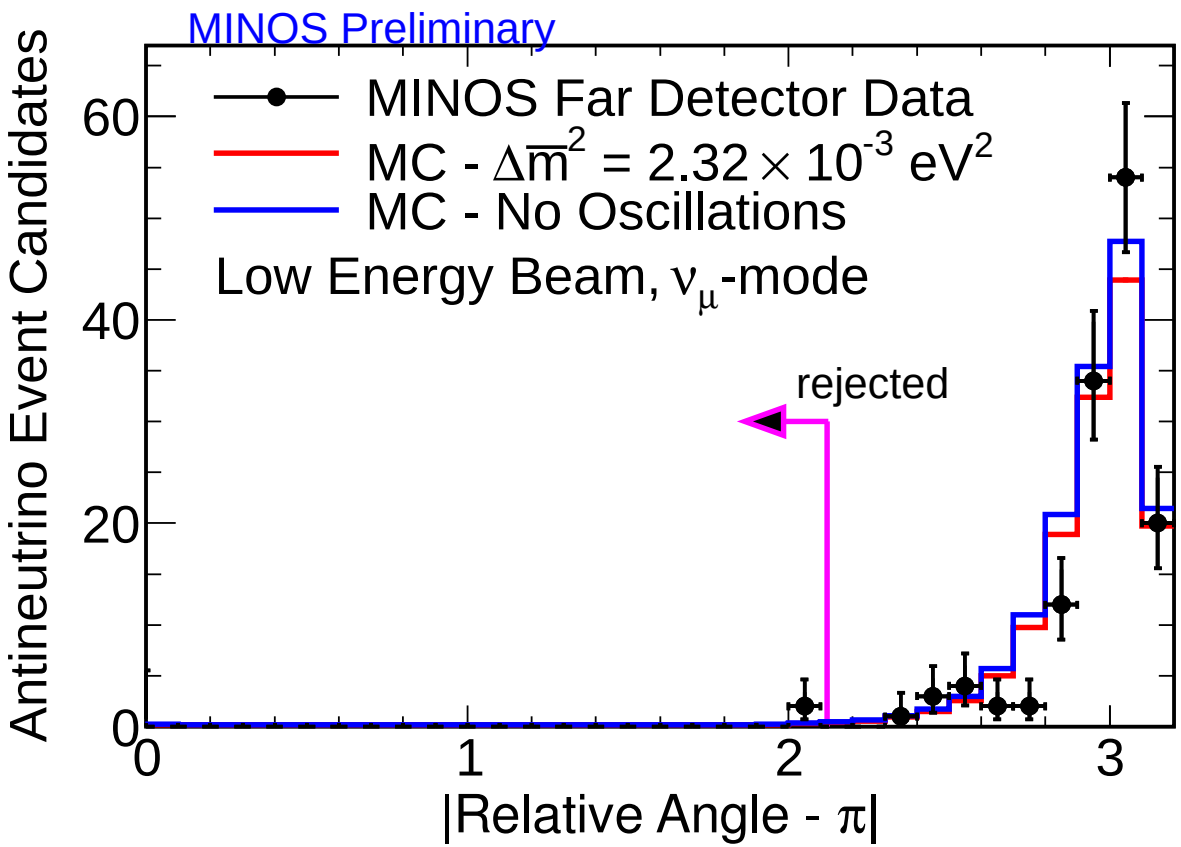

Figure 13: $|\mathrm{RelativeAngle} - \pi|$ distribution of selected $\overline{\nu}_\mu$ events in the Far Detector passing all other selection criteria. The red histogram represents the Monte Carlo expectation with current best fit oscillation parameters, the blue histogram represents the no oscillations expectation and black points represent data. Monte Carlo is normalized to data corresponding to an exposure of 7.1×10^{20} protons on target.

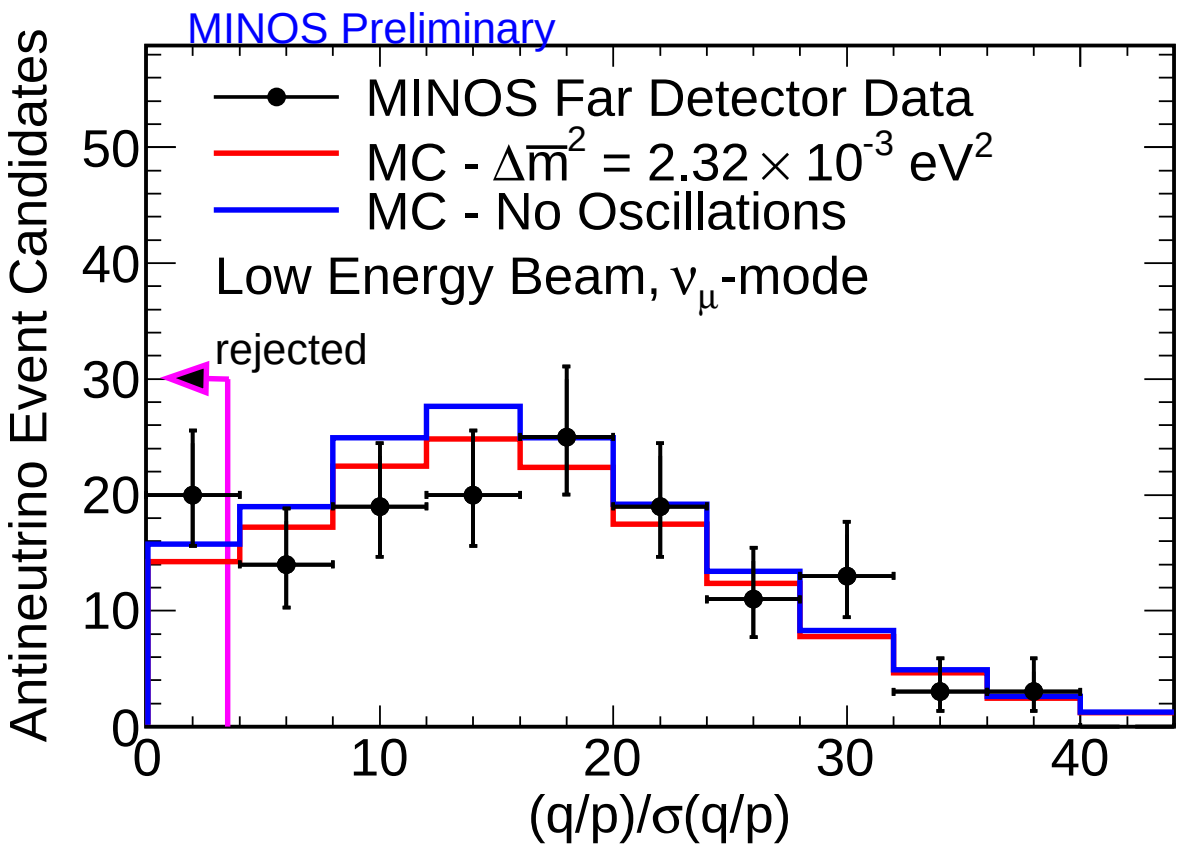

Figure 14: $(q/p)/\sigma(q/p)$ *track charge sign significance* distribution of Far Detector events before the charge sign significance cut for events passing all other selection criteria. The red histogram represents the Monte Carlo expectation with current best fit oscillation parameters, the blue histogram represents the no oscillations case, and black points represent data. Monte Carlo is normalized to data corresponding to an exposure of 7.1×10^{20} protons on target.

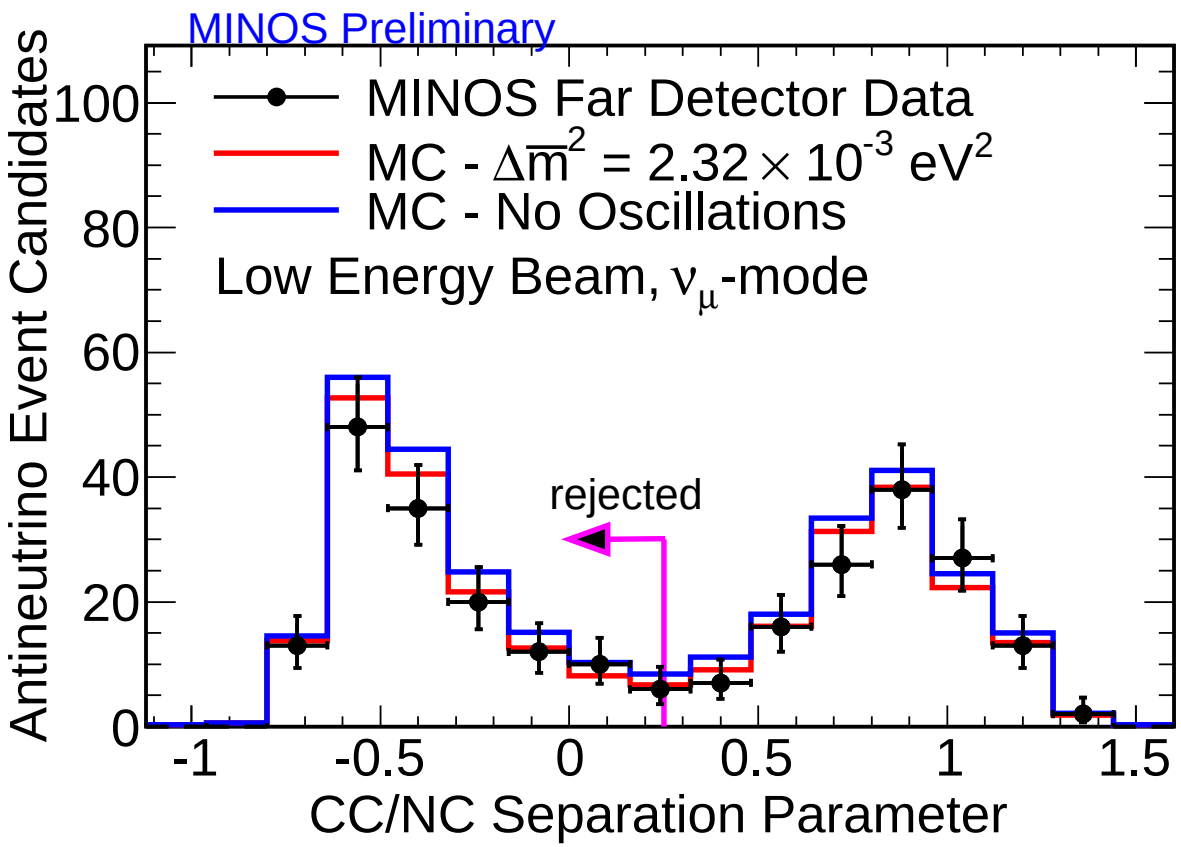

Figure 15: Distribution of the CC/NC separation parameter of events passing all other selection criteria. The red histogram represents the Monte Carlo expectation with current best fit oscillation parameters, the blue histogram represents the no oscillations case, and black points represent data. Monte Carlo is normalized to data corresponding to an exposure of 7.1×10^{20} protons on target.

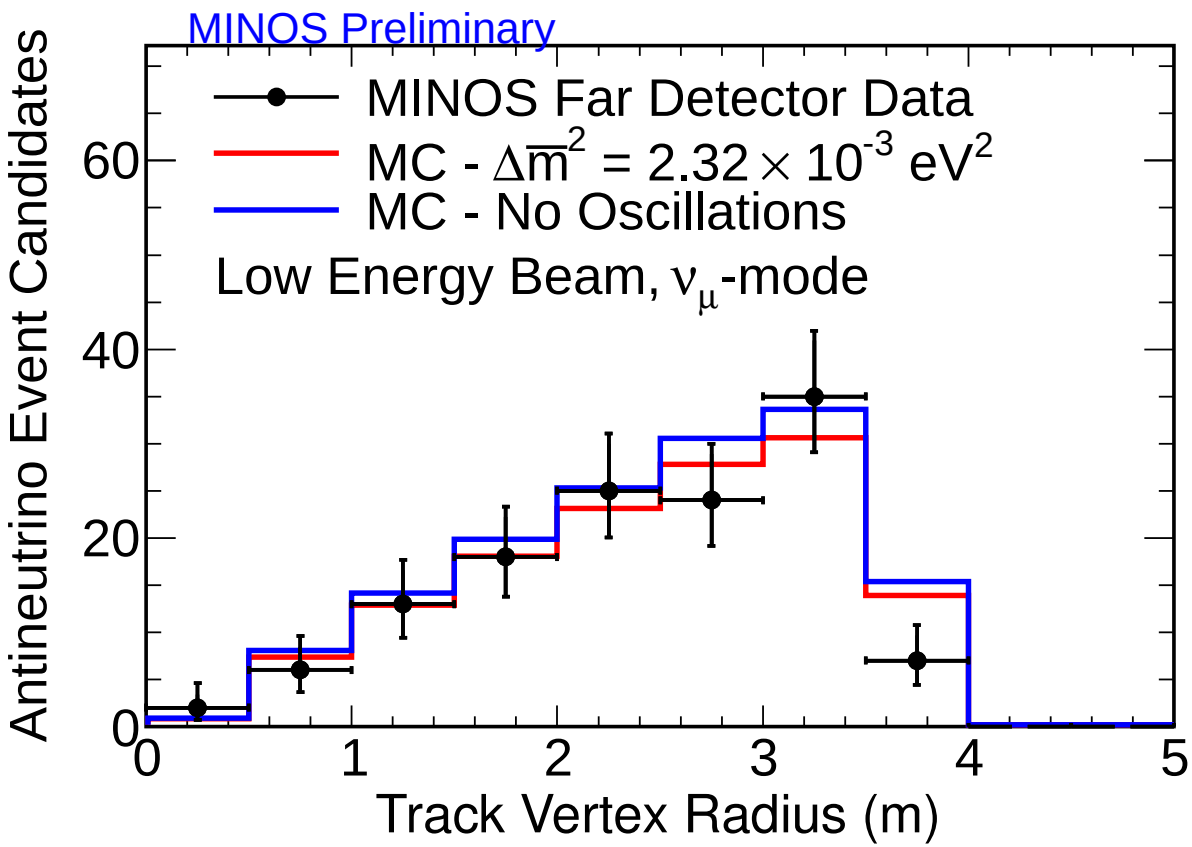

Figure 16: Track vertex radius distribution of selected $\overline{\nu}_\mu$ events in the Far Detector. The red histogram represents the Monte Carlo expectation with current best fit oscillation parameters, the blue histogram represents the no oscillations expectation and black points represent data. Monte Carlo is normalized to data corresponding to an exposure of 7.1×10^{20} protons on target.

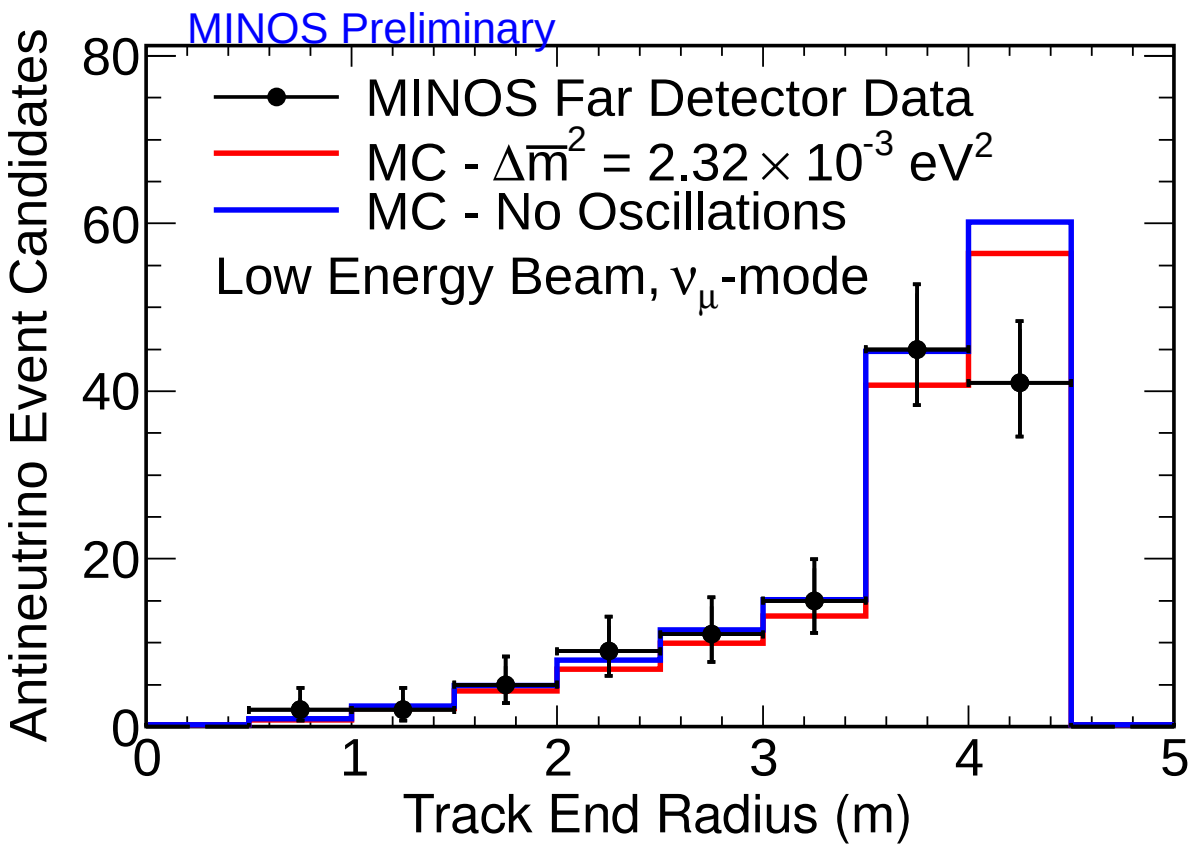

Figure 17: Track end radius distribution of selected $\overline{\nu}_\mu$ events in the Far Detector. The red histogram represents the Monte Carlo expectation with current best fit oscillation parameters, the blue histogram represents the no oscillations expectation and black points represent data. Monte Carlo is normalized to data corresponding to an exposure of 7.1×10^{20} protons on target.

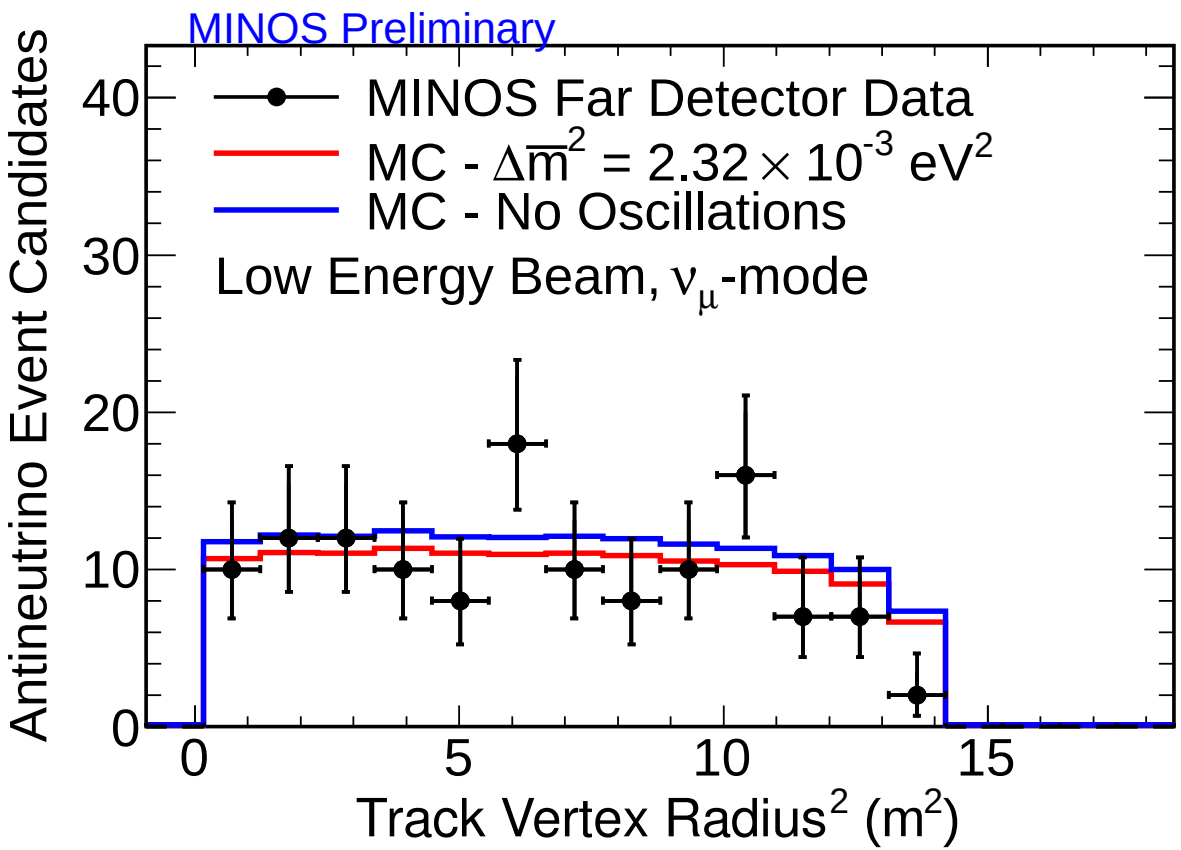

Figure 18: Track vertex radius^2 distribution of selected $\overline{\nu}_\mu$ events in the Far Detector. The red histogram represents the Monte Carlo expectation with the best fit oscillation parameters, the blue histogram represents the no oscillations expectation and black points represent data. Monte Carlo is normalized to data corresponding to an exposure of 7.1×10^{20} protons on target.

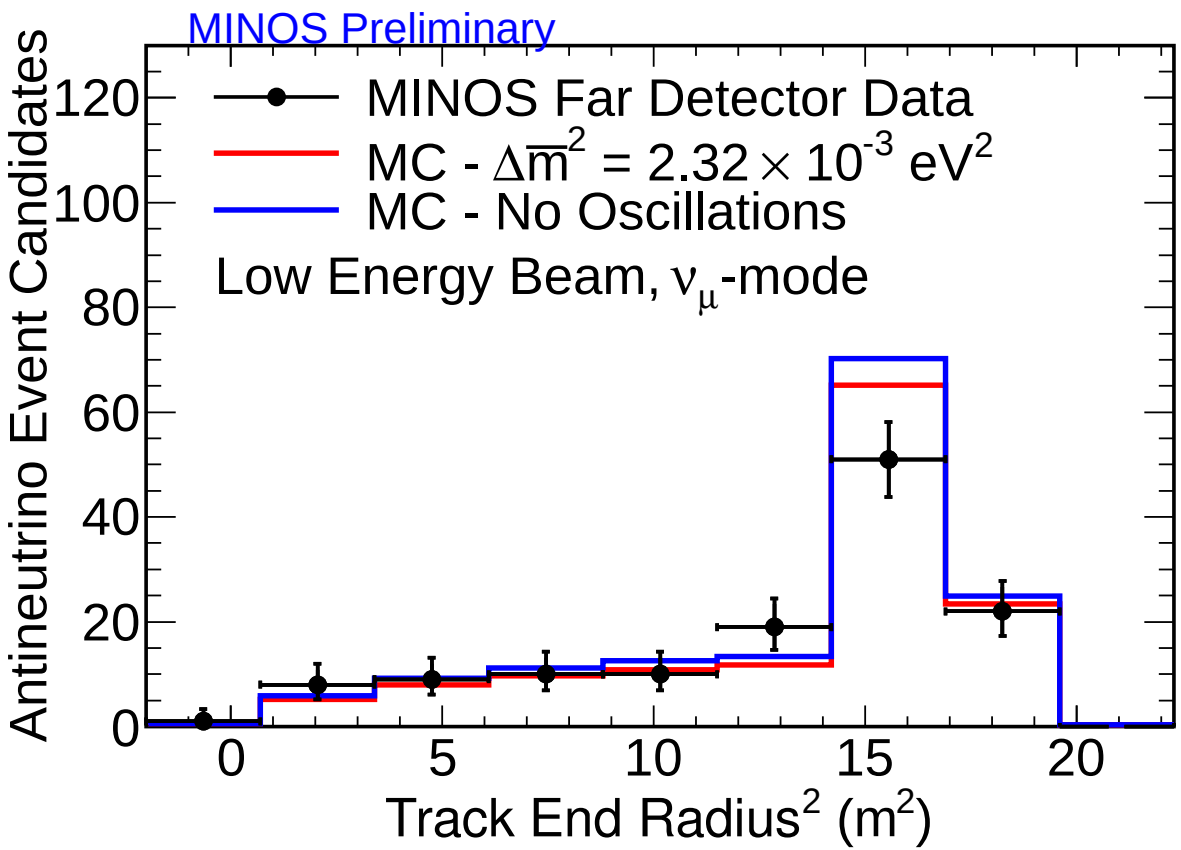

Figure 19: Track end radius^2 distribution of selected $\overline{\nu}_\mu$ events in the Far Detector. The red histogram represents the Monte Carlo expectation with the best fit oscillation parameters, the blue histogram represents the no oscillations expectation and black points represent data. Monte Carlo is normalized to data corresponding to an exposure of 7.1×10^{20} protons on target.

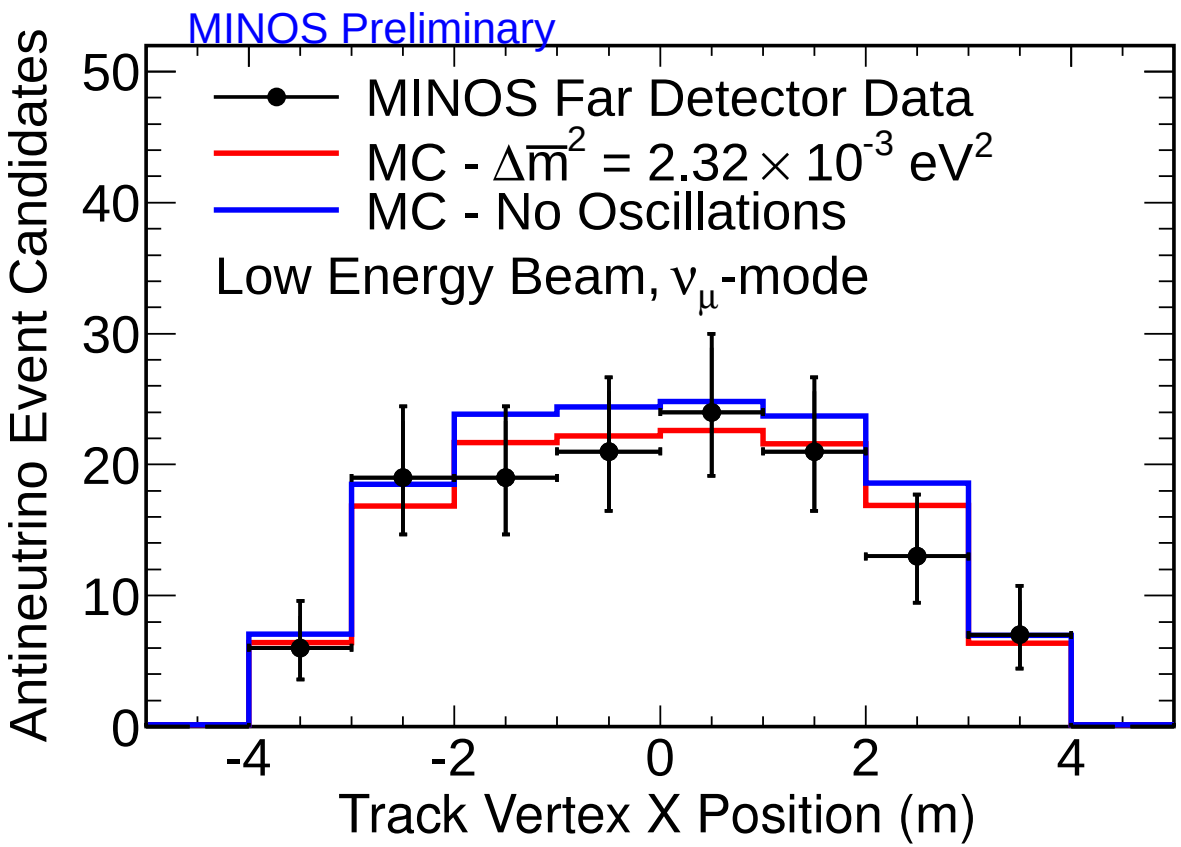

Figure 20: Track vertex X position distribution of selected $\overline{\nu}_\mu$ events in the Far Detector. The red histogram represents the Monte Carlo expectation with current best fit oscillation parameters, the blue histogram represents the no oscillations expectation and black points represent data. Monte Carlo is normalized to data corresponding to an exposure of 7.1×10^{20} protons on target.

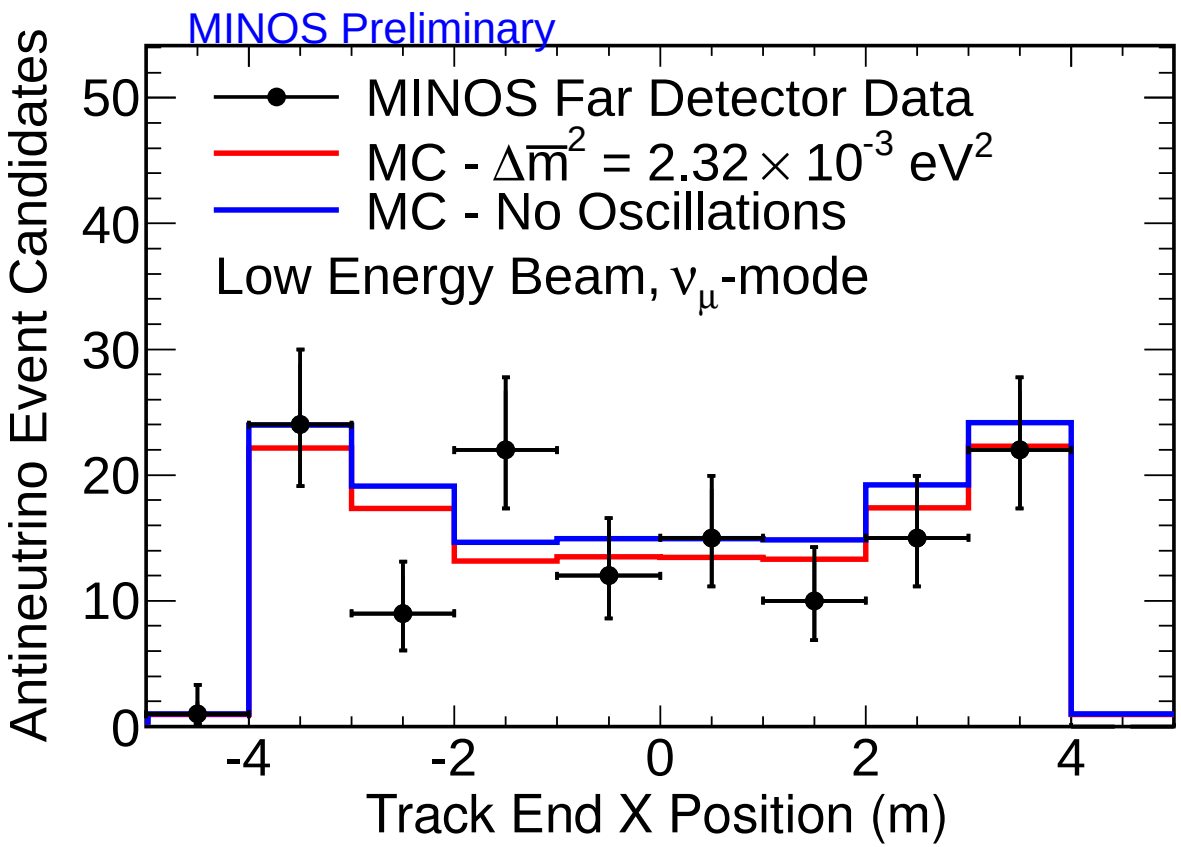

Figure 21: Track end X position distribution of selected $\overline{\nu}_\mu$ events in the Far Detector. The red histogram represents the Monte Carlo expectation with current best fit oscillation parameters, the blue histogram represents the no oscillations expectation and black points represent data. Monte Carlo is normalized to data corresponding to an exposure of 7.1×10^{20} protons on target.

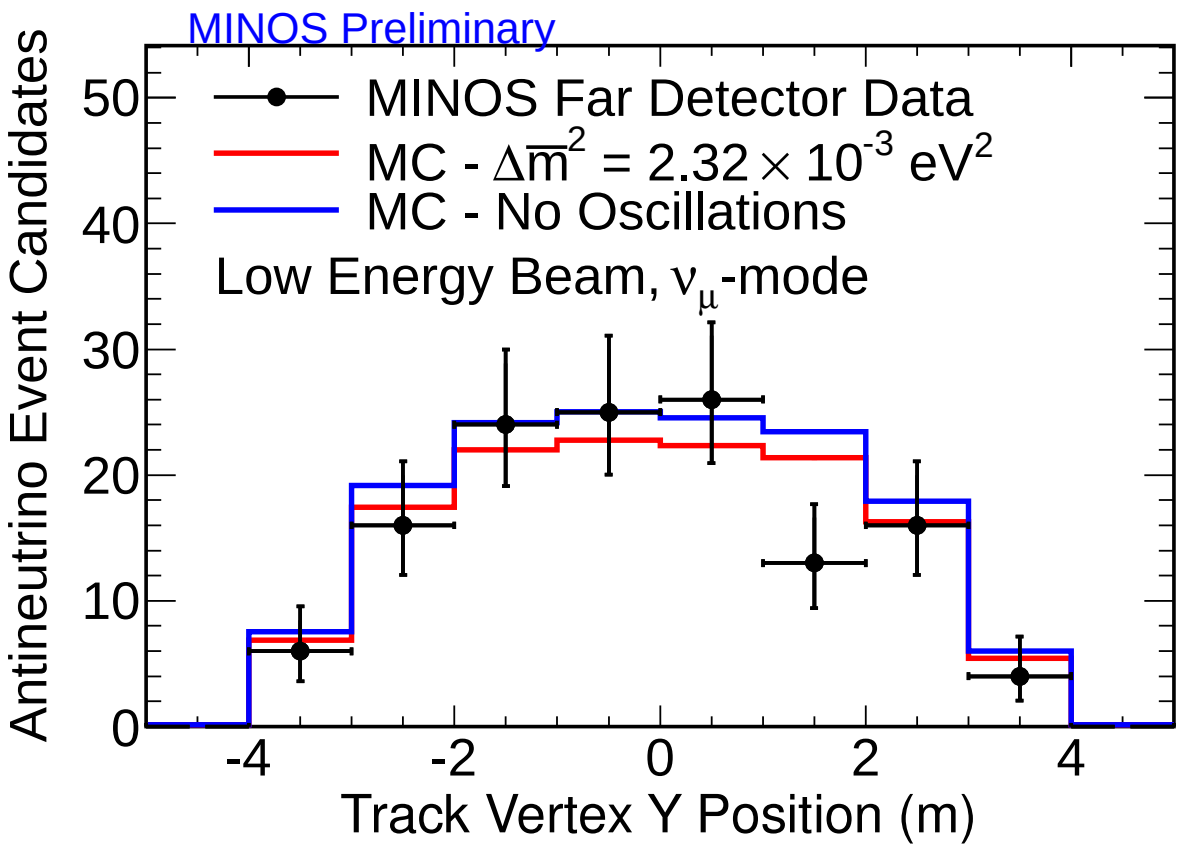

Figure 22: Track vertex Y position distribution of selected $\overline{\nu}_\mu$ events in the Far Detector. The red histogram represents the Monte Carlo expectation with current best fit oscillation parameters, the blue histogram represents the no oscillations expectation and black points represent data. Monte Carlo is normalized to data corresponding to an exposure of 7.1×10^{20} protons on target.

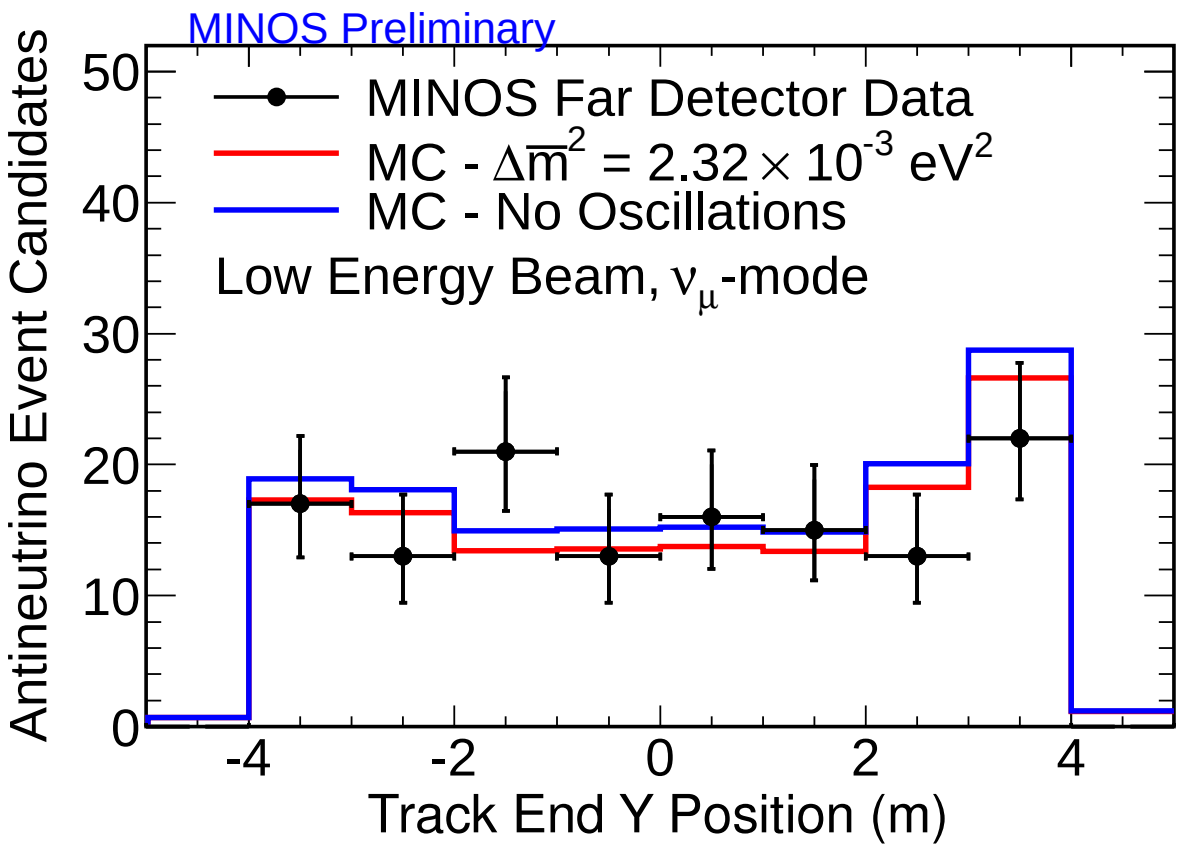

Figure 23: Track end Y position distribution of selected $\overline{\nu}_\mu$ events in the Far Detector. The red histogram represents the Monte Carlo expectation with current best fit oscillation parameters, the blue histogram represents the no oscillations expectation and black points represent data. Monte Carlo is normalized to data corresponding to an exposure of 7.1×10^{20} protons on target.

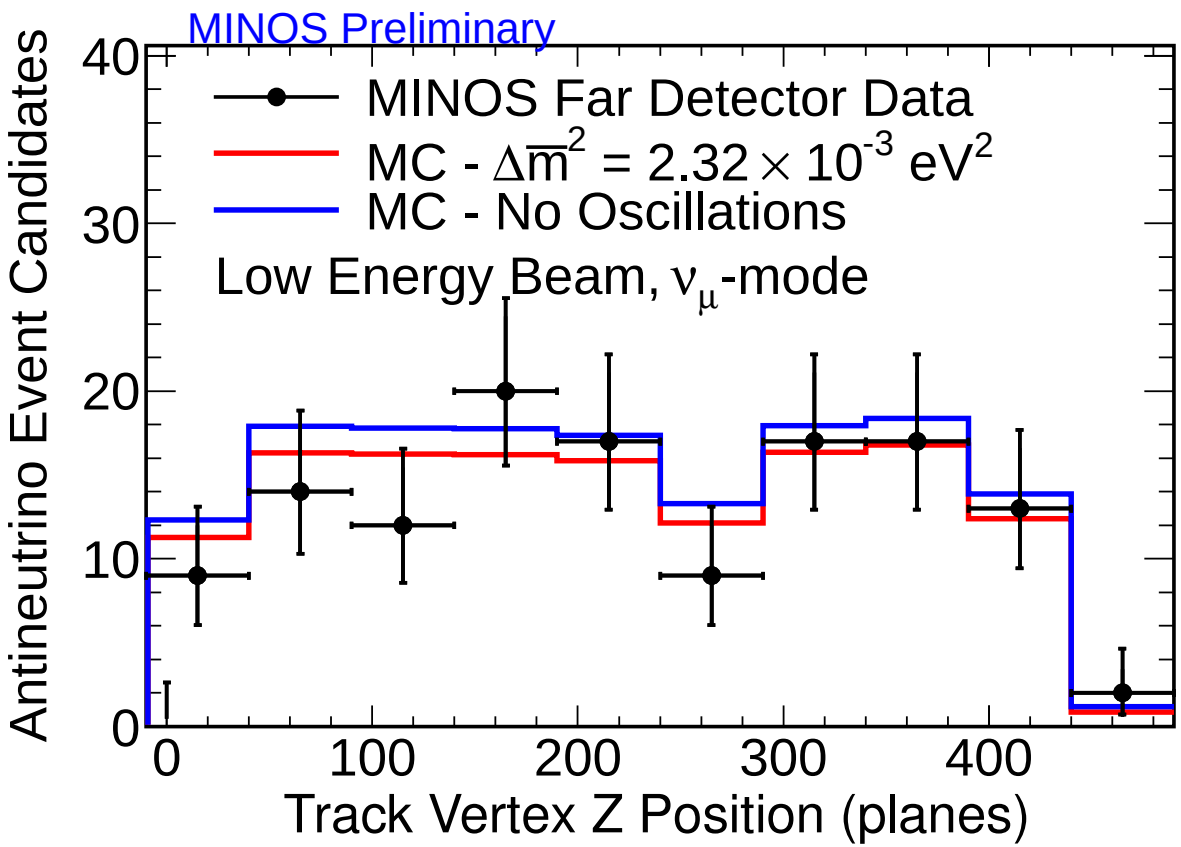

Figure 24: Track vertex longitudinal position distribution of selected $\overline{\nu}_\mu$ events in the Far Detector. The red histogram represents the Monte Carlo expectation with the best fit oscillation parameters, the blue histogram represents the no oscillations expectation and black points represent data. Monte Carlo is normalized to data corresponding to an exposure of 7.1×10^{20} protons on target.

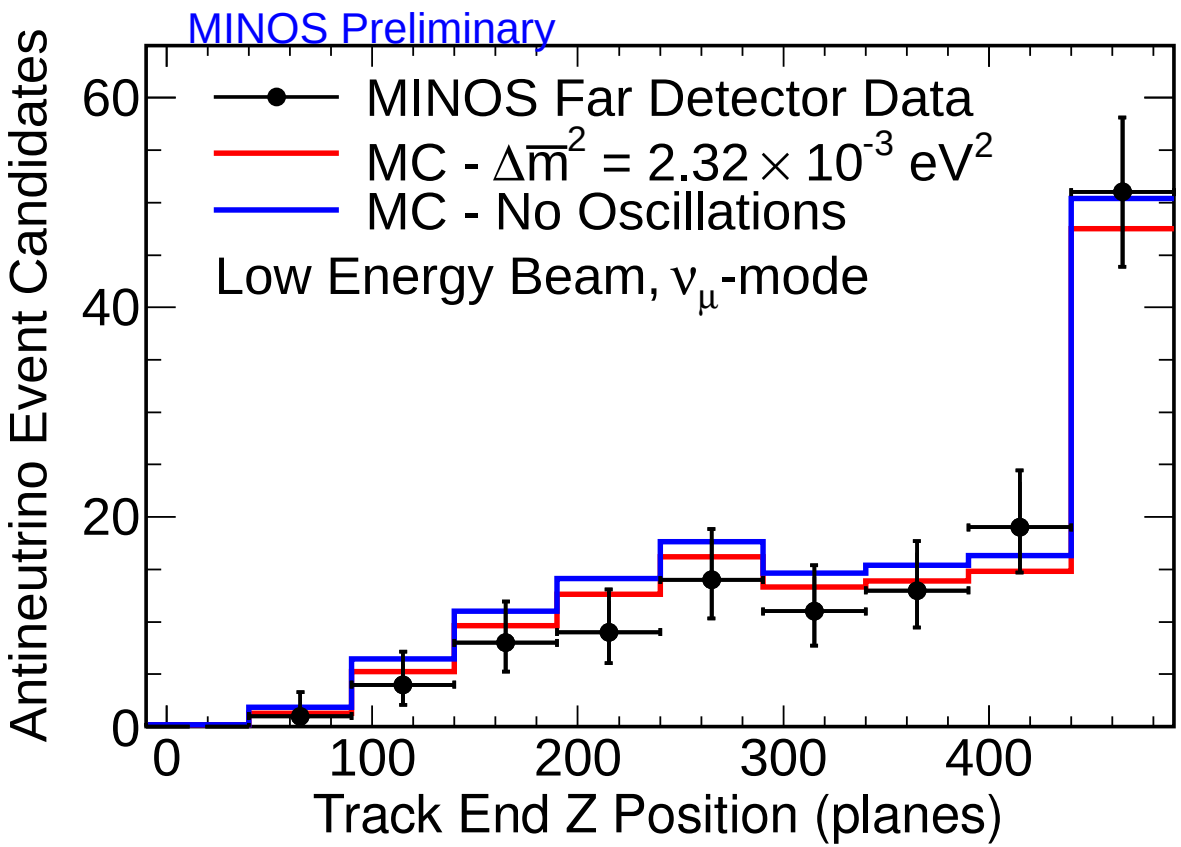

Figure 25: Track end longitudinal position distribution of selected $\overline{\nu}_\mu$ events in the Far Detector. The red histogram represents the Monte Carlo expectation with the best fit oscillation parameters, the blue histogram represents the no oscillations expectation and black points represent data. Monte Carlo is normalized to data corresponding to an exposure of 7.1×10^{20} protons on target.

Systematics and FD stability

minos-doc-7136

minos-doc-7195

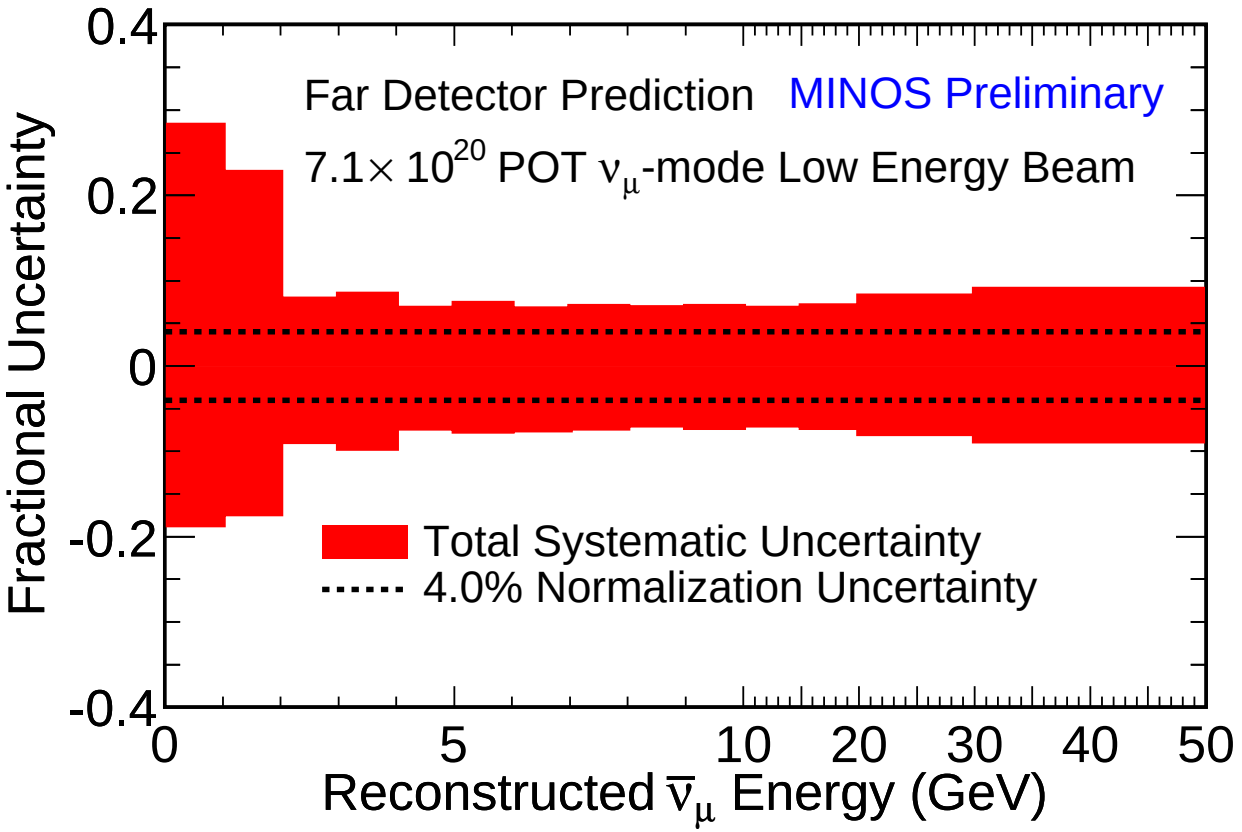

Figure 26: The total systematic band on the far detector prediction includes the effect of all sources of systematic uncertainty added in quadrature.

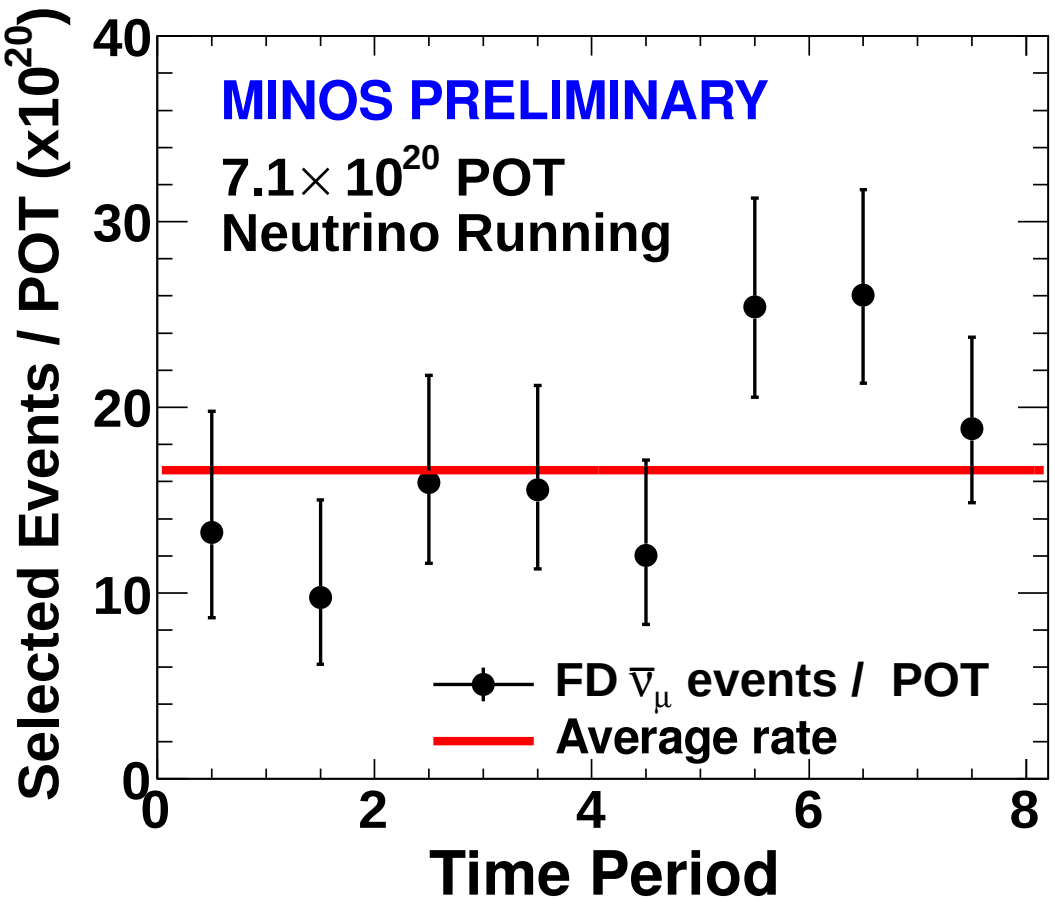

Figure 27: The FD event rate (normalized by exposure), as a function of time over runs 1–3. The division of the data into 8 periods is arbitrary: the aim of the plot is to show the effect over time. Essentially, the first 4 bins are RunI+II and the last four bins are RunIII.

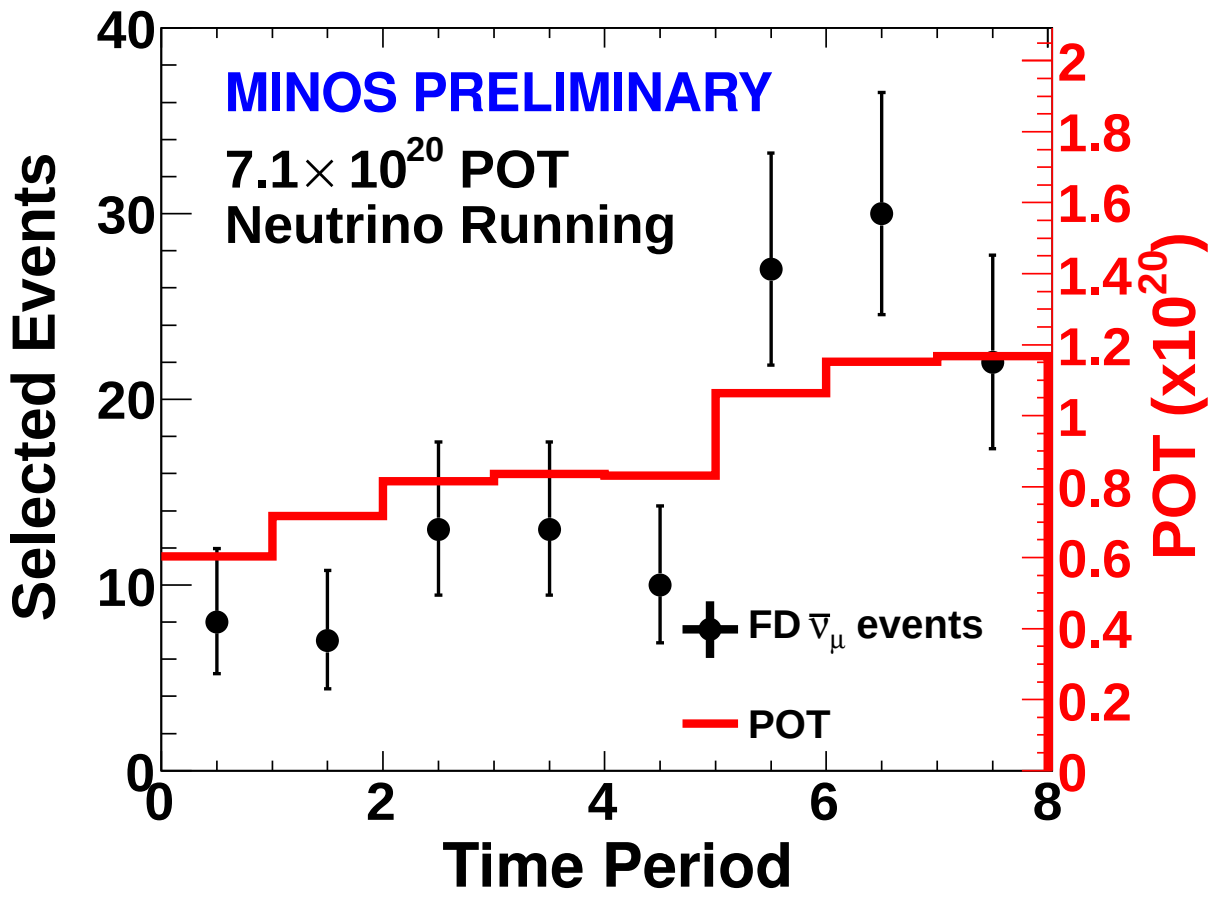

Figure 28: The nuber of selected FD CC $\overline{\nu}_\mu$ events as a function of time, compared to the number of PoT recorded in each time period. The figure covers the LE data in runs 1–3. The division of the data into 8 periods is arbitrary: the aim of the plot is to show the effect over time. Essentially, the first 4 bins are RunI+II and the last four bins are RunIII.

Oscillation Results

minos-doc-7973

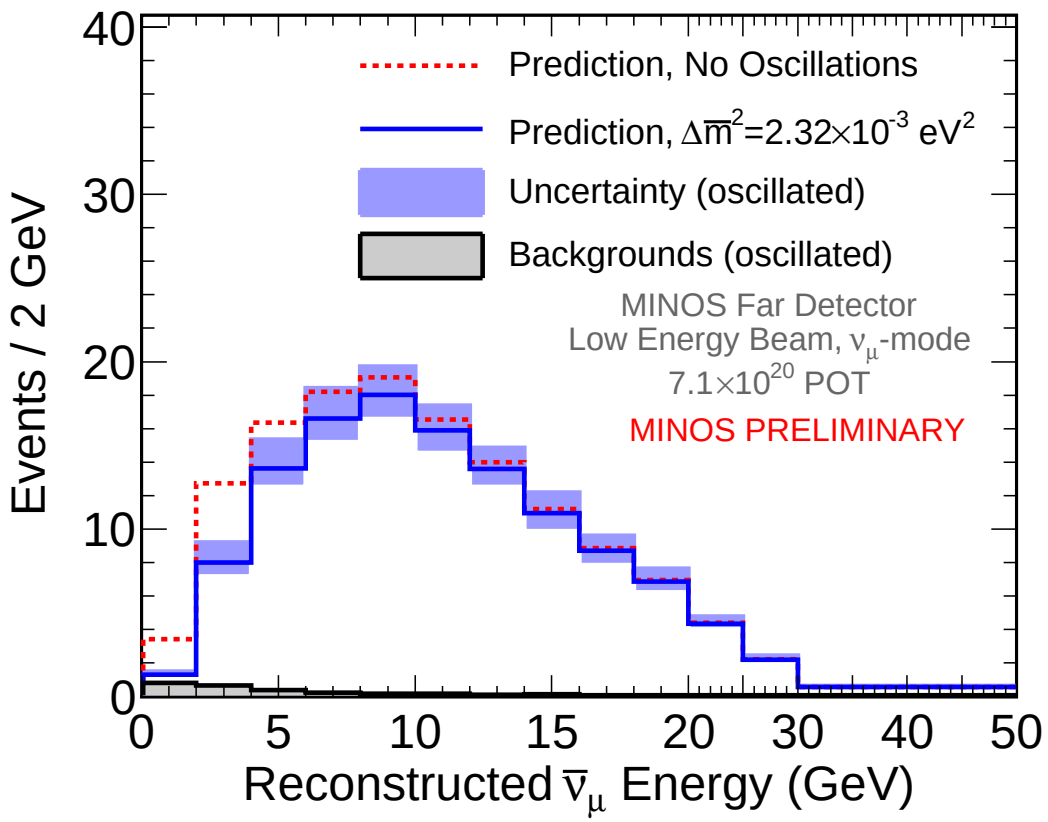

Figure 29: Far detector numubar predictions with no oscillations (red histogram) and with oscillations at the 2011 neutrino best fit parameters (blue histogram). The band around the oscillated prediction represents the total systematic uncertainty. Total background in the oscillated prediction is also displayed (gray shaded histogram). The predictions correspond to an exposure of 7.1×10^{20} POT.

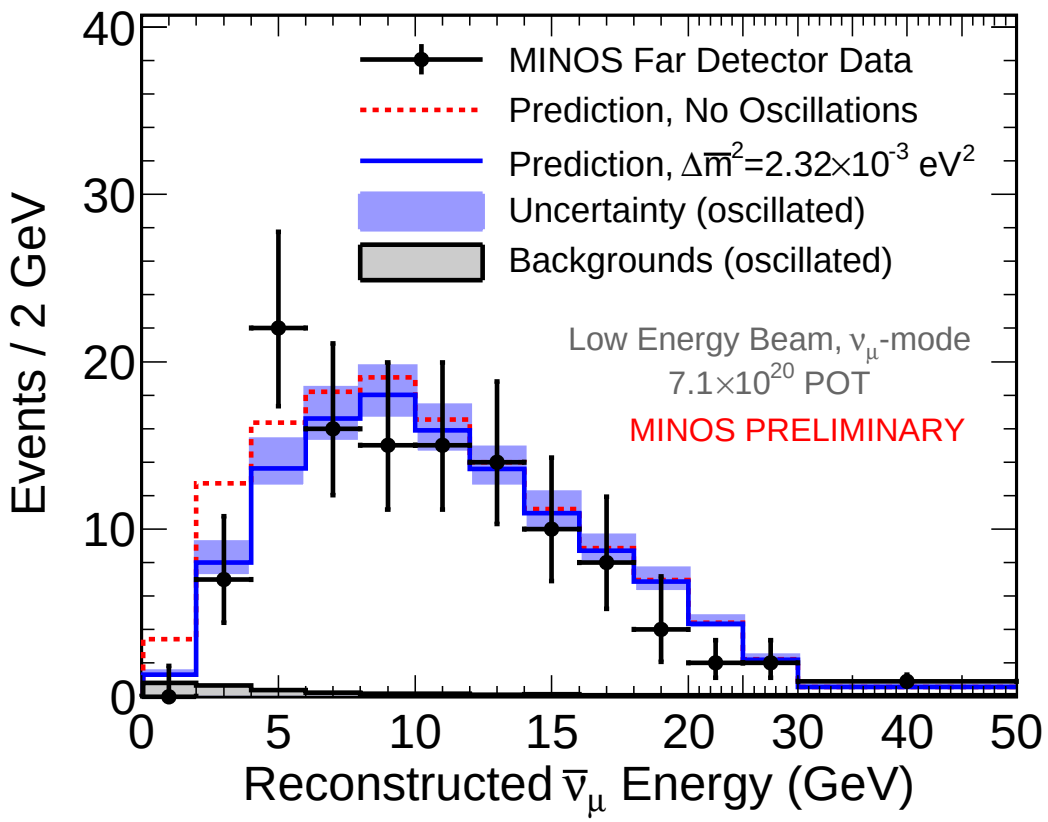

Figure 30: Far detector numubar data (black points) and predictions with no oscillations (red histogram) and with oscillations at the 2011 neutrino best fit parameters (blue histogram). The band around the oscillated prediction represents the total systematic uncertainty. Total background in the oscillated prediction is also displayed (gray shaded histogram). The data and predictions correspond to an exposure of 7.1×10^{20} POT.

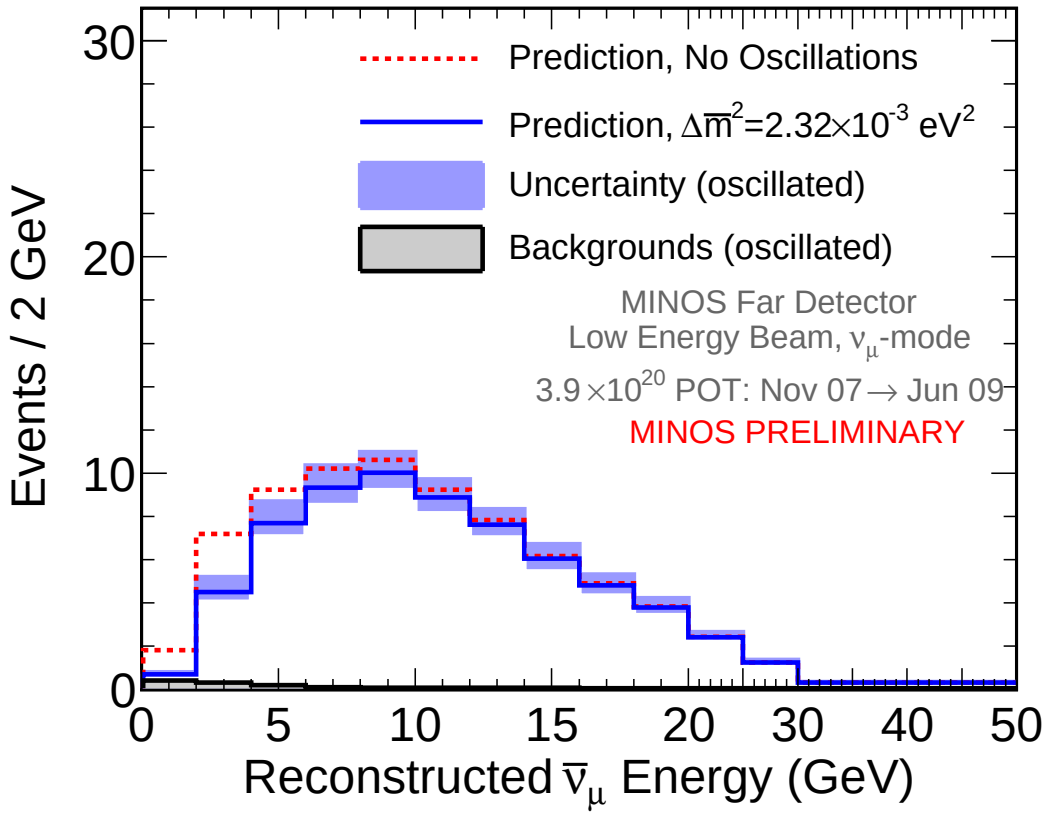

Figure 31: Far detector numubar predictions with no oscillations (red histogram) and with oscillations at the 2011 neutrino best fit parameters (blue histogram). The band around the oscillated prediction represents the total systematic uncertainty. Total background in the oscillated prediction is also displayed (gray shaded histogram). The predictions correspond to an exposure of 3.9×10^{20} POT.

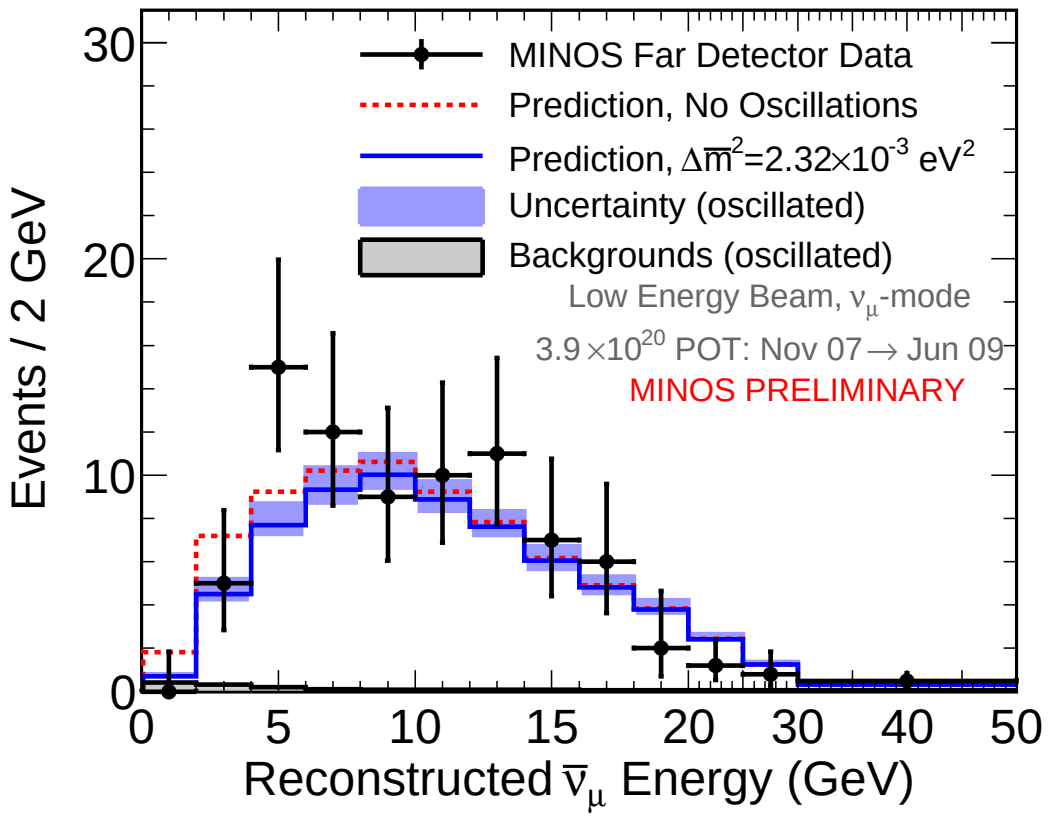

Figure 32: Far detector numubar data (black points) and predictions with no oscillations (red histogram) and with oscillations at the 2011 neutrino best fit parameters (blue histogram). The band around the oscillated prediction represents the total systematic uncertainty. Total background in the oscillated prediction is also displayed (gray shaded histogram). The data and predictions correspond to an exposure of 3.9×10^{20} POT.

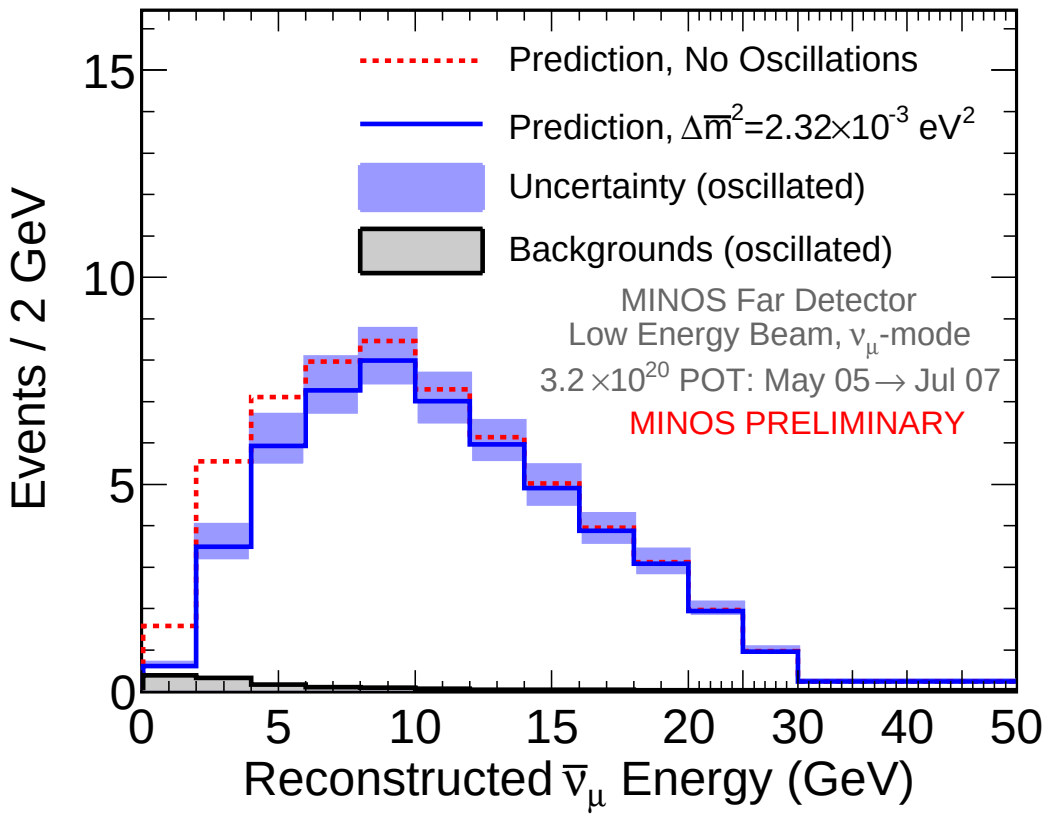

Figure 33: Far detector numubar predictions with no oscillations (red histogram) and with oscillations at the 2011 neutrino best fit parameters (blue histogram). The band around the oscillated prediction represents the total systematic uncertainty. Total background in the oscillated prediction is also displayed (gray shaded histogram). The predictions correspond to an exposure of 3.2×10^{20} POT.

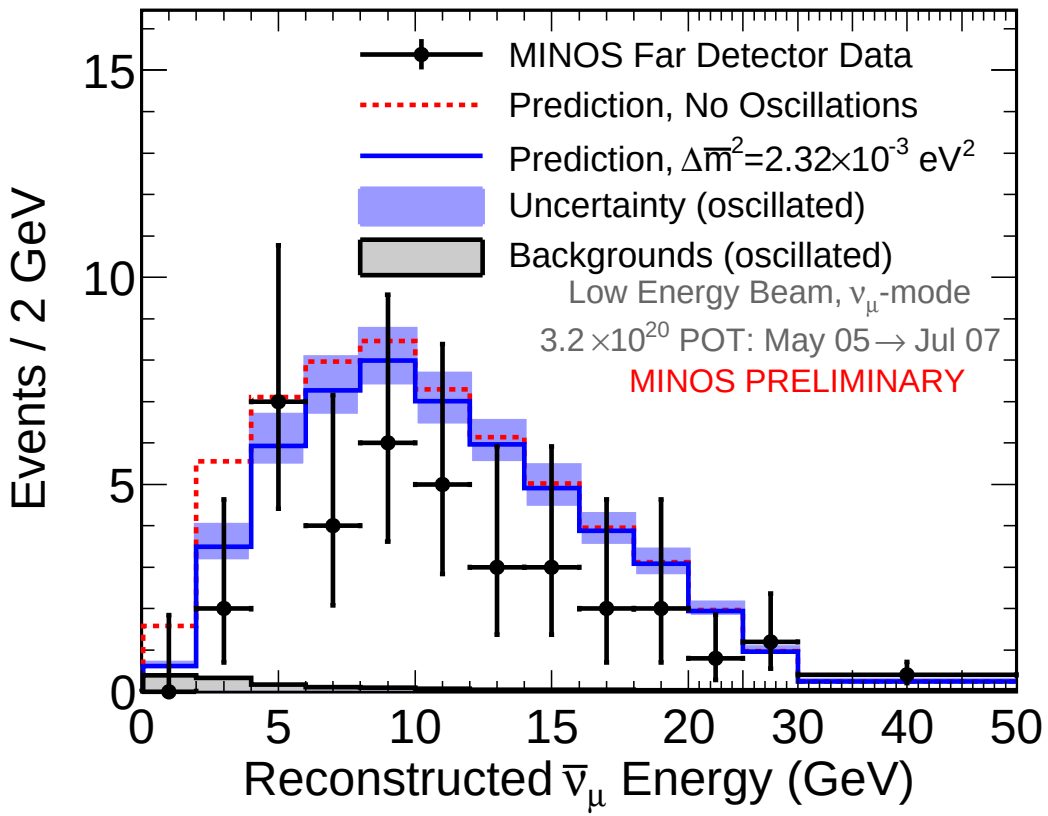

Figure 34: Far detector numubar data (black points) and predictions with no oscillations (red histogram) and with oscillations at the 2011 neutrino best fit parameters (blue histogram). The band around the oscillated prediction represents the total systematic uncertainty. Total background in the oscillated prediction is also displayed (gray shaded histogram). The data and predictions correspond to an exposure of 3.2×10^{20} POT.

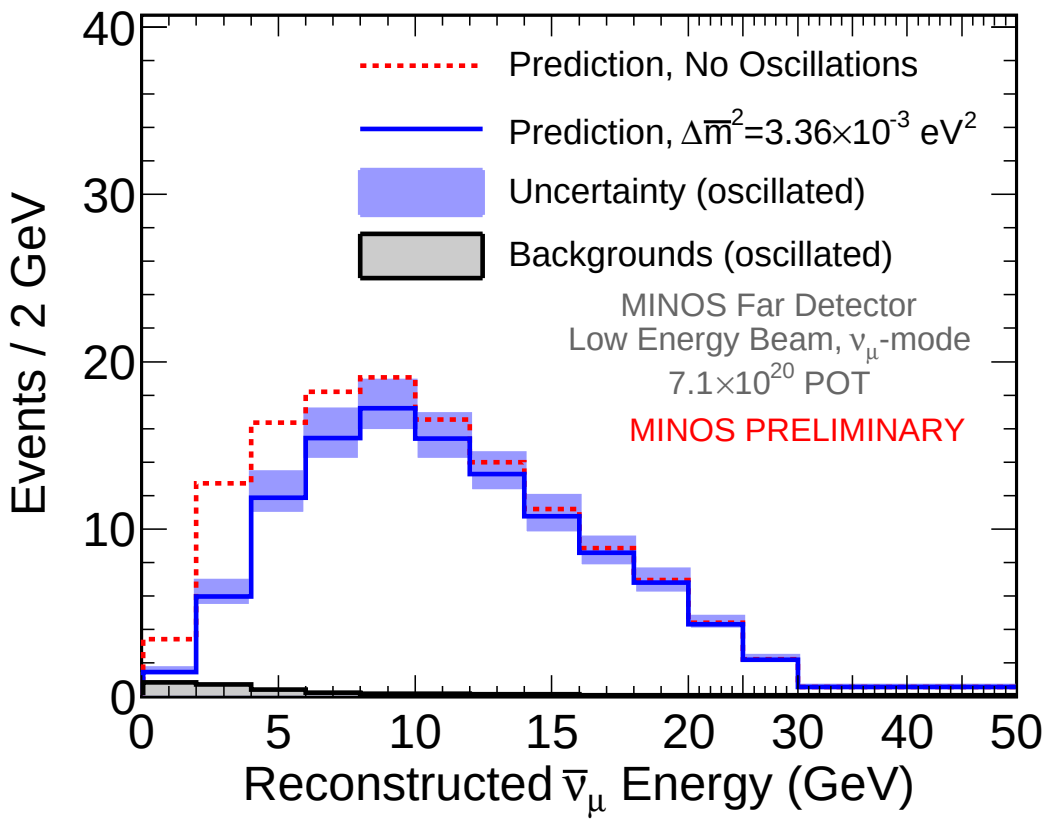

Figure 35: Far detector numubar predictions with no oscillations (red histogram) and with oscillations at the 2010 antineutrino best fit parameters (blue histogram). The band around the oscillated prediction represents the total systematic uncertainty. Total background in the oscillated prediction is also displayed (gray shaded histogram). The predictions correspond to an exposure of 7.1×10^{20} POT.

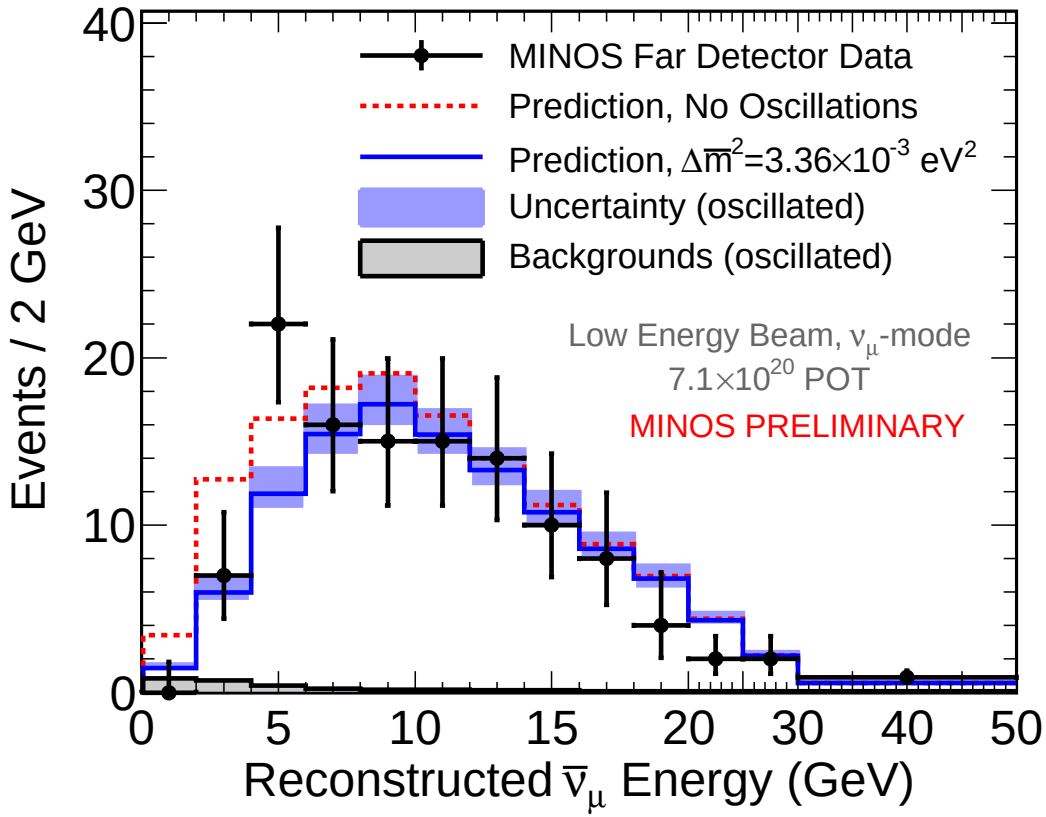

Figure 36: Far detector numubar data (black points) and predictions with no oscillations (red histogram) and with oscillations at the 2010 antineutrino best fit parameters (blue histogram). The band around the oscillated prediction represents the total systematic uncertainty. Total background in the oscillated prediction is also displayed (gray shaded histogram). The data and predictions correspond to an exposure of 7.1×10^{20} POT.

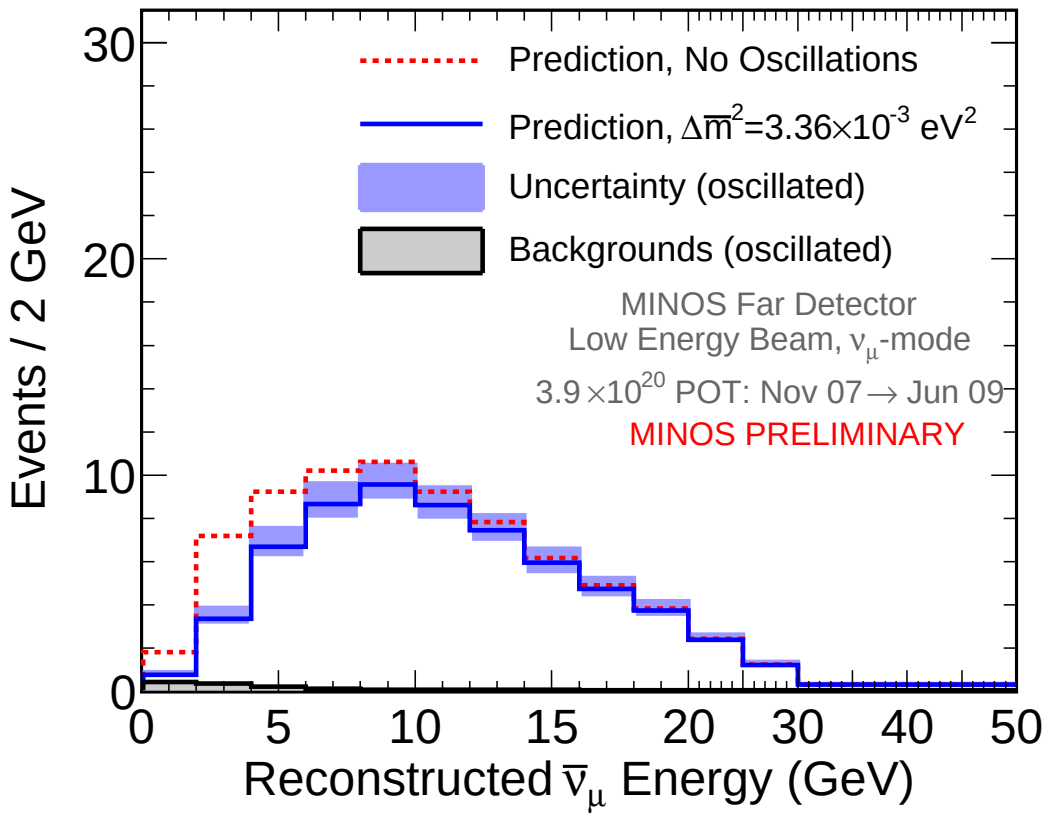

Figure 37: Far detector numubar predictions with no oscillations (red histogram) and with oscillations at the 2010 antineutrino best fit parameters (blue histogram). The band around the oscillated prediction represents the total systematic uncertainty. Total background in the oscillated prediction is also displayed (gray shaded histogram). The predictions correspond to an exposure of 3.9×10^{20} POT.

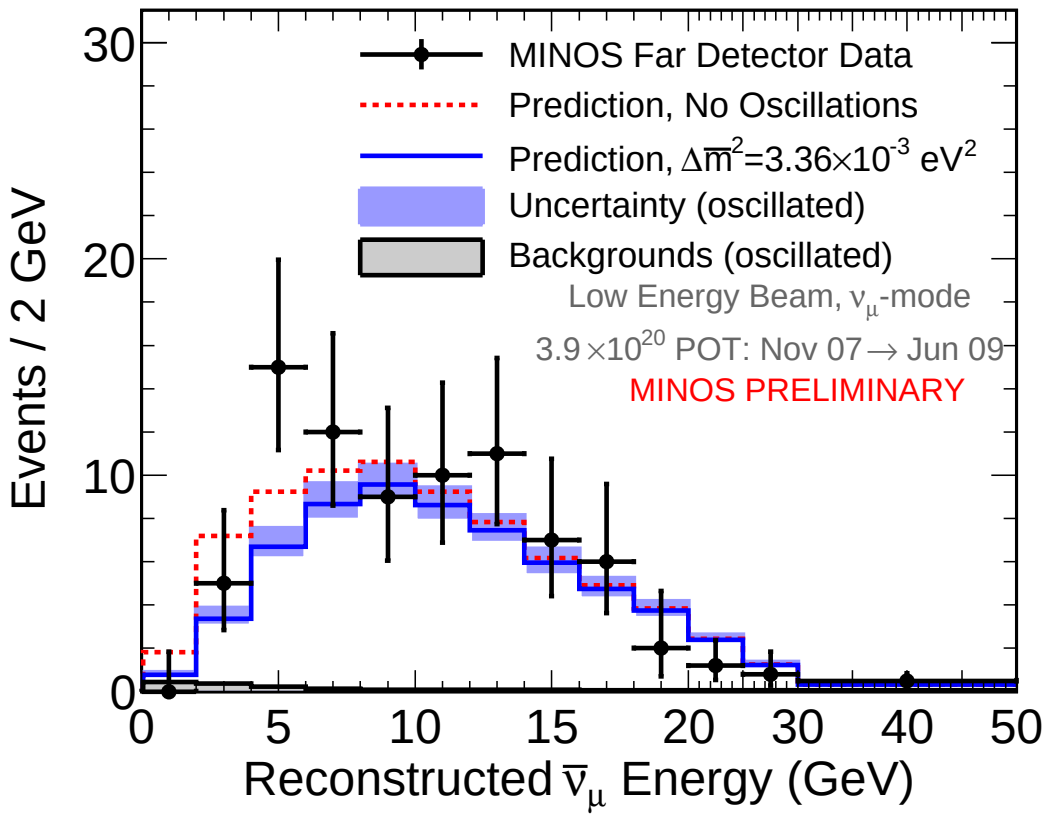

Figure 38: Far detector numubar data (black points) and predictions with no oscillations (red histogram) and with oscillations at the 2010 antineutrino best fit parameters (blue histogram). The band around the oscillated prediction represents the total systematic uncertainty. Total background in the oscillated prediction is also displayed (gray shaded histogram). The data and predictions correspond to an exposure of 3.9×10^{20} POT.

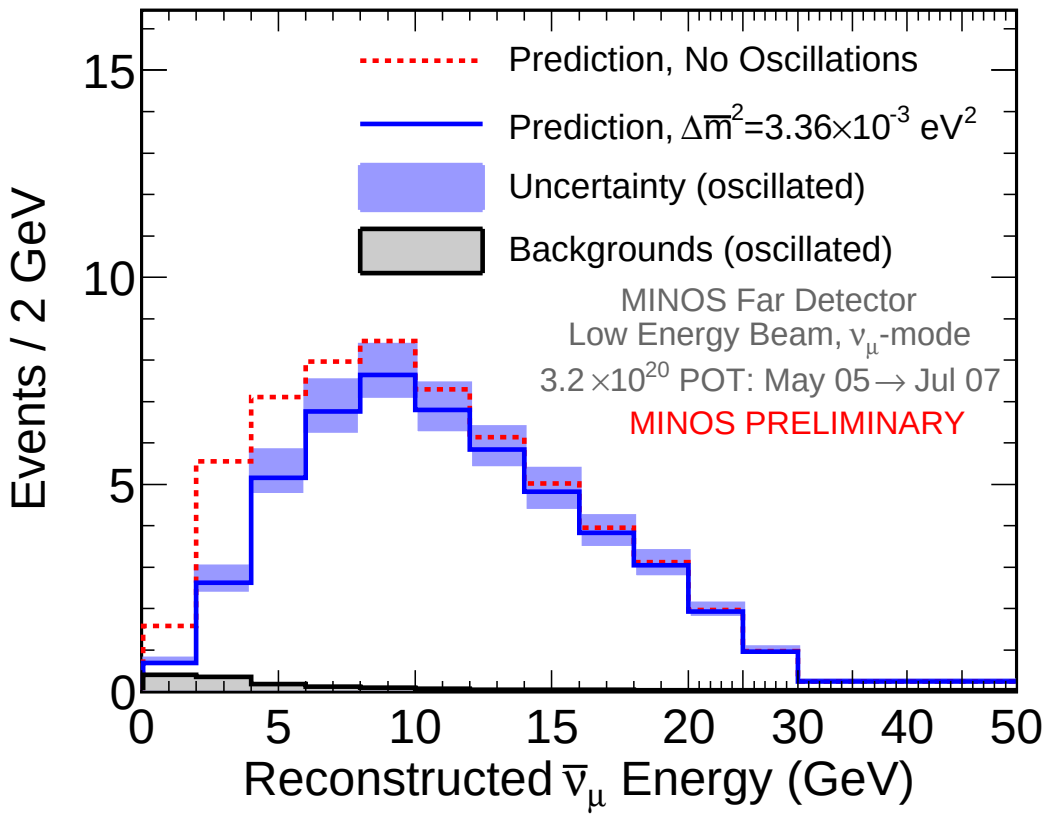

Figure 39: Far detector numubar predictions with no oscillations (red histogram) and with oscillations at the 2010 antineutrino best fit parameters (blue histogram). The band around the oscillated prediction represents the total systematic uncertainty. Total background in the oscillated prediction is also displayed (gray shaded histogram). The predictions correspond to an exposure of 3.2×10^{20} POT.

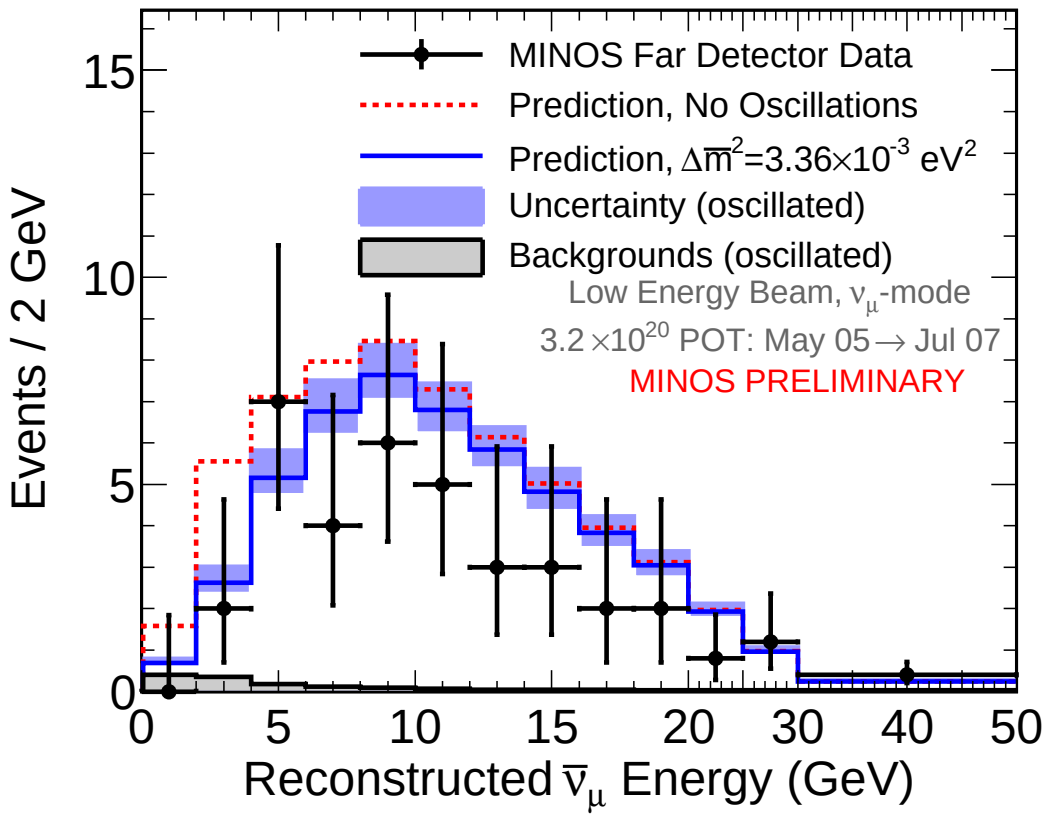

Figure 40: Far detector numubar data (black points) and predictions with no oscillations (red histogram) and with oscillations at the 2010 antineutrino best fit parameters (blue histogram). The band around the oscillated prediction represents the total systematic uncertainty. Total background in the oscillated prediction is also displayed (gray shaded histogram). The data and predictions correspond to an exposure of 3.2×10^{20} POT.

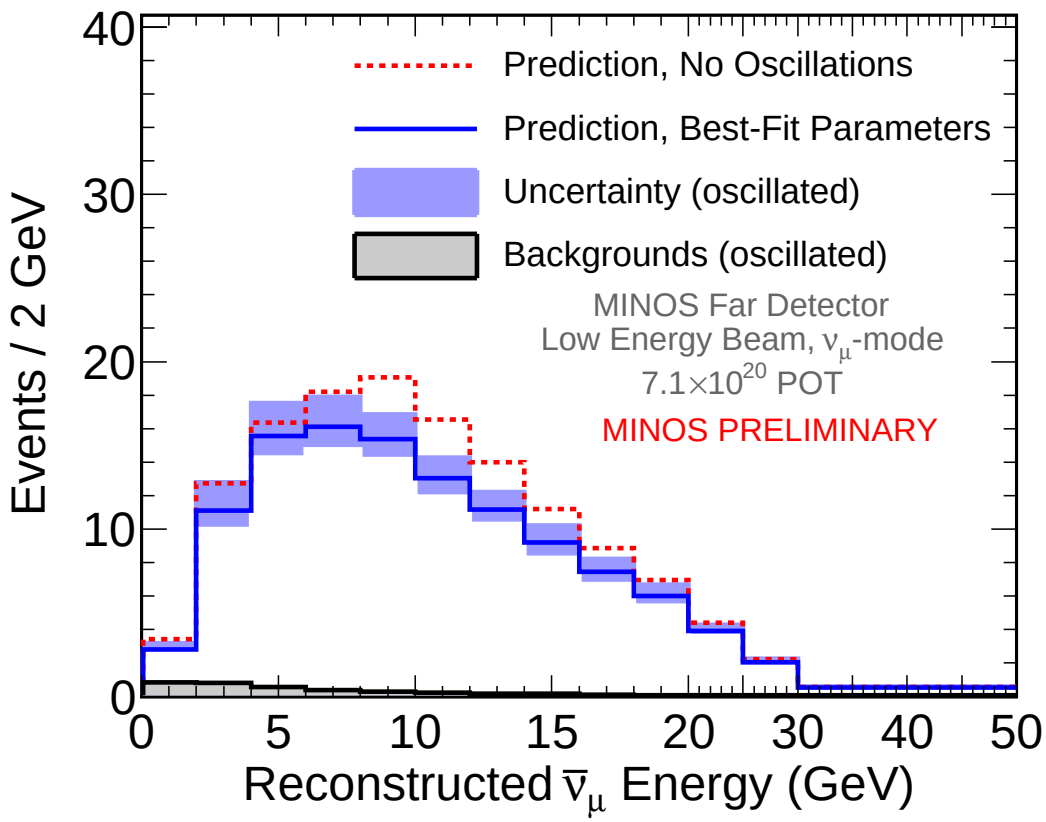

Figure 41: Far detector numubar predictions with no oscillations (red histogram) and with the best-fit oscillation parameters (blue histogram). The band around the oscillated prediction represents the total systematic uncertainty. Total background in the oscillated prediction is also displayed (gray shaded histogram). The predictions correspond to an exposure of 7.1×10^{20} POT.

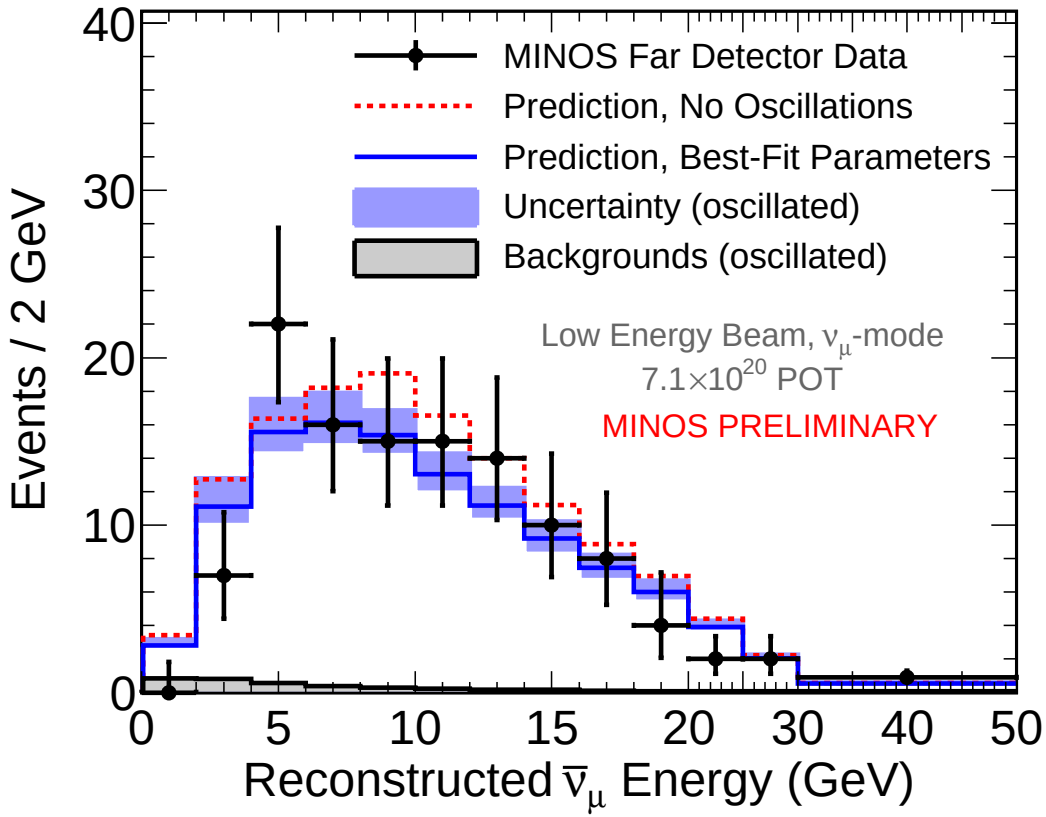

Figure 42: Far detector numubar data and predictions with no oscillations (red histogram) and with the best-fit oscillation parameters (blue histogram). The band around the oscillated prediction represents the total systematic uncertainty. Total background in the oscillated prediction is also displayed (gray shaded histogram). The data and predictions correspond to an exposure of 7.1×10^{20} POT.

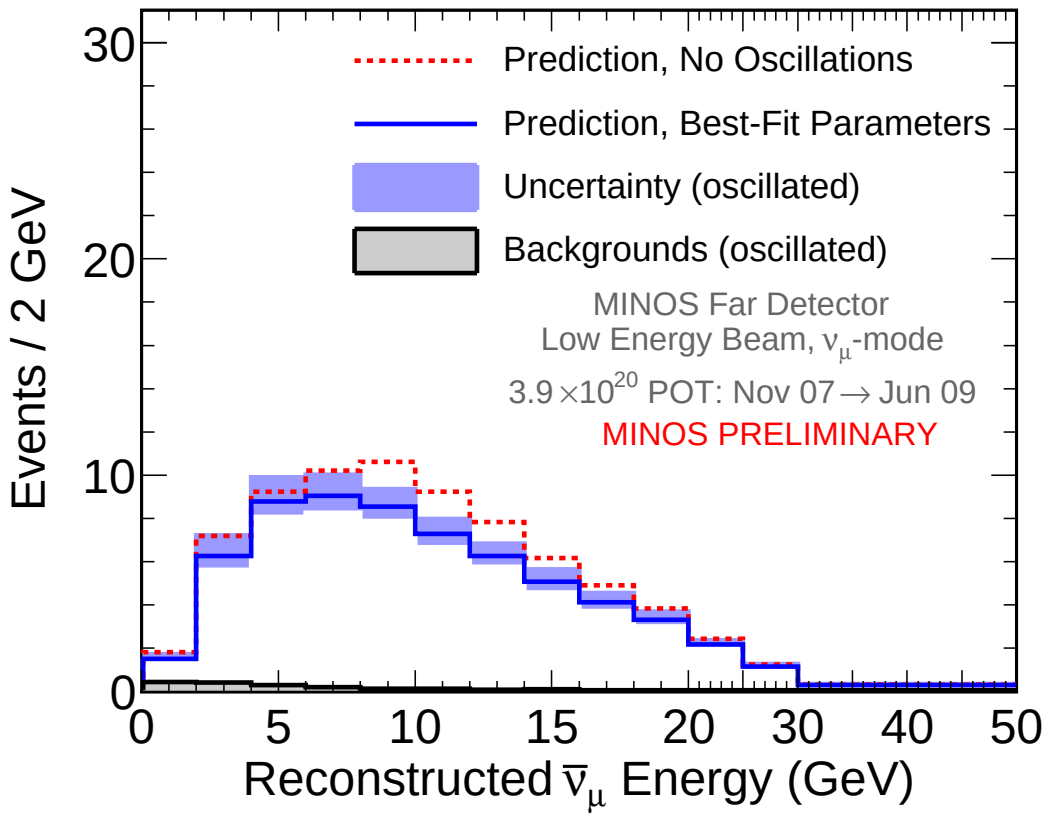

Figure 43: Far detector numubar predictions with no oscillations (red histogram) and with the best-fit oscillation parameters (blue histogram). The band around the oscillated prediction represents the total systematic uncertainty. Total background in the oscillated prediction is also displayed (gray shaded histogram). The predictions correspond to an exposure of 3.9×10^{20} POT.

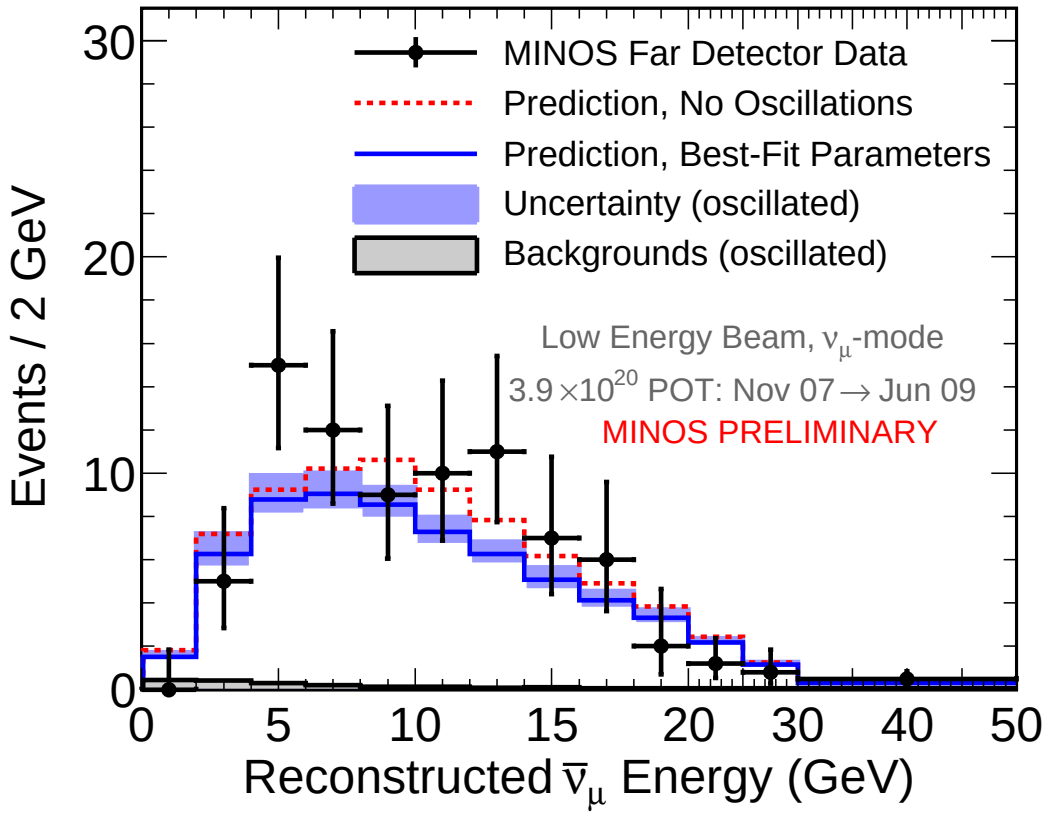

Figure 44: Far detector numubar data and predictions with no oscillations (red histogram) and with the best-fit oscillation parameters (blue histogram). The band around the oscillated prediction represents the total systematic uncertainty. Total background in the oscillated prediction is also displayed (gray shaded histogram). The data and predictions correspond to an exposure of 3.9×10^{20} POT.

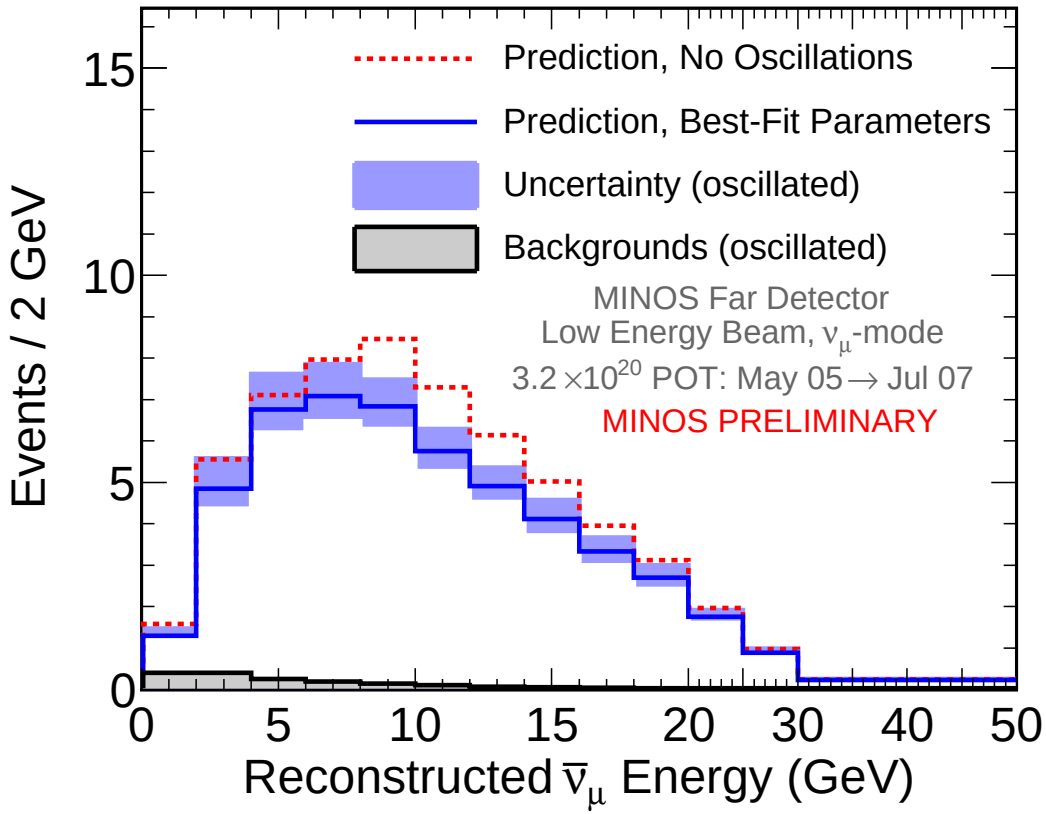

Figure 45: Far detector numubar predictions with no oscillations (red histogram) and with the best-fit oscillation parameters (blue histogram). The band around the oscillated prediction represents the total systematic uncertainty. Total background in the oscillated prediction is also displayed (gray shaded histogram). The predictions correspond to an exposure of 3.2×10^{20} POT.

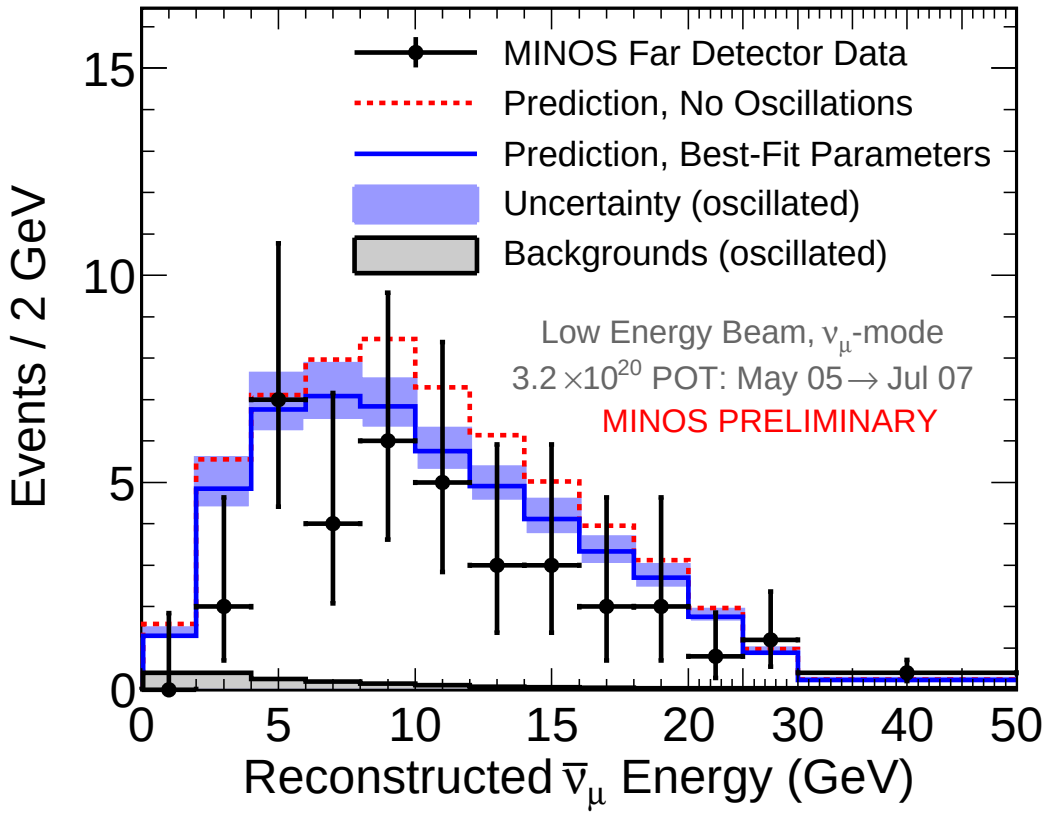

Figure 46: Far detector numubar data and predictions with no oscillations (red histogram) and with the best-fit oscillation parameters (blue histogram). The band around the oscillated prediction represents the total systematic uncertainty. Total background in the oscillated prediction is also displayed (gray shaded histogram). The data and predictions correspond to an exposure of 3.2×10^{20} POT.

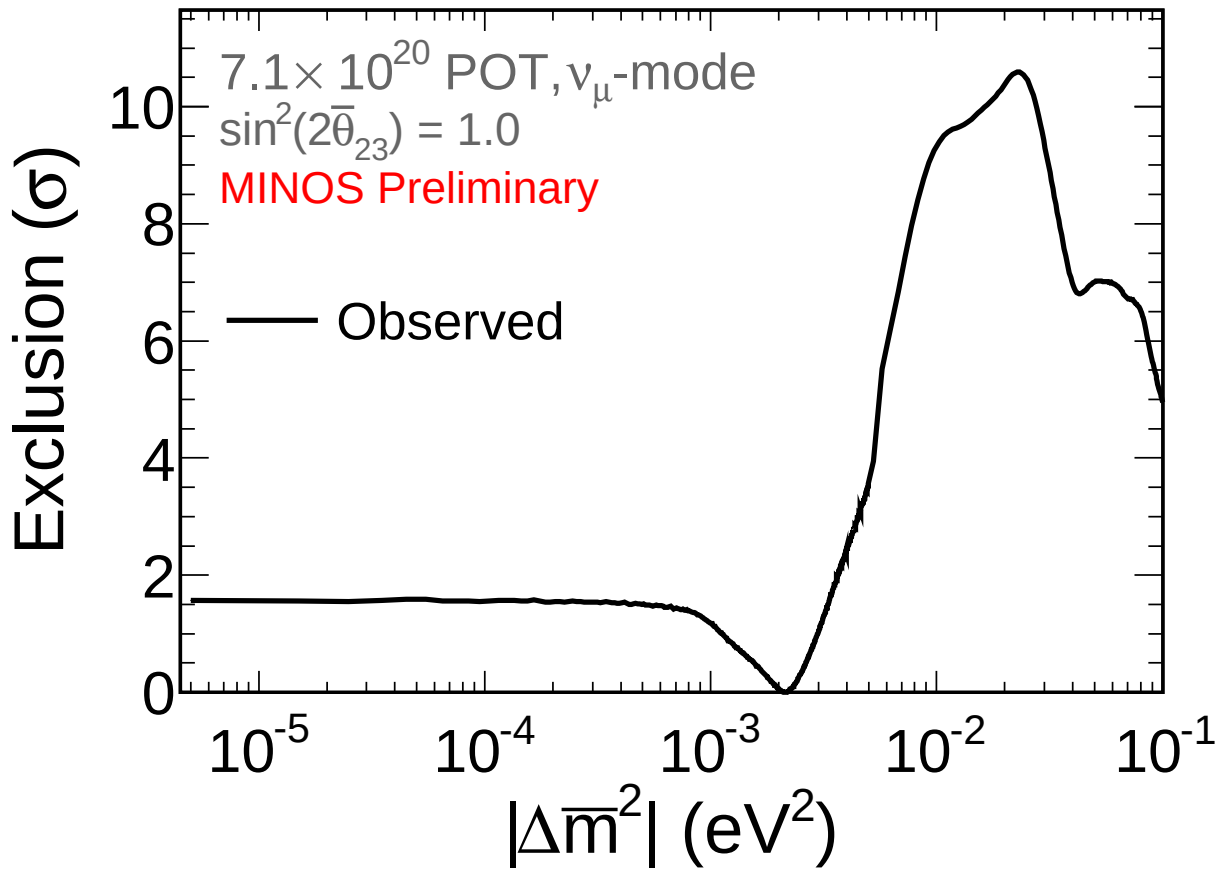

Figure 47: One-dimensional fit of $\Delta\bar{m}^2$ at maximal mixing, showing the values excluded by this result. At maximal mixing, we exclude $\Delta\bar{m}^2 > 4.49 \times 10^{-3}$ eV^2 at a 3 σ significance.

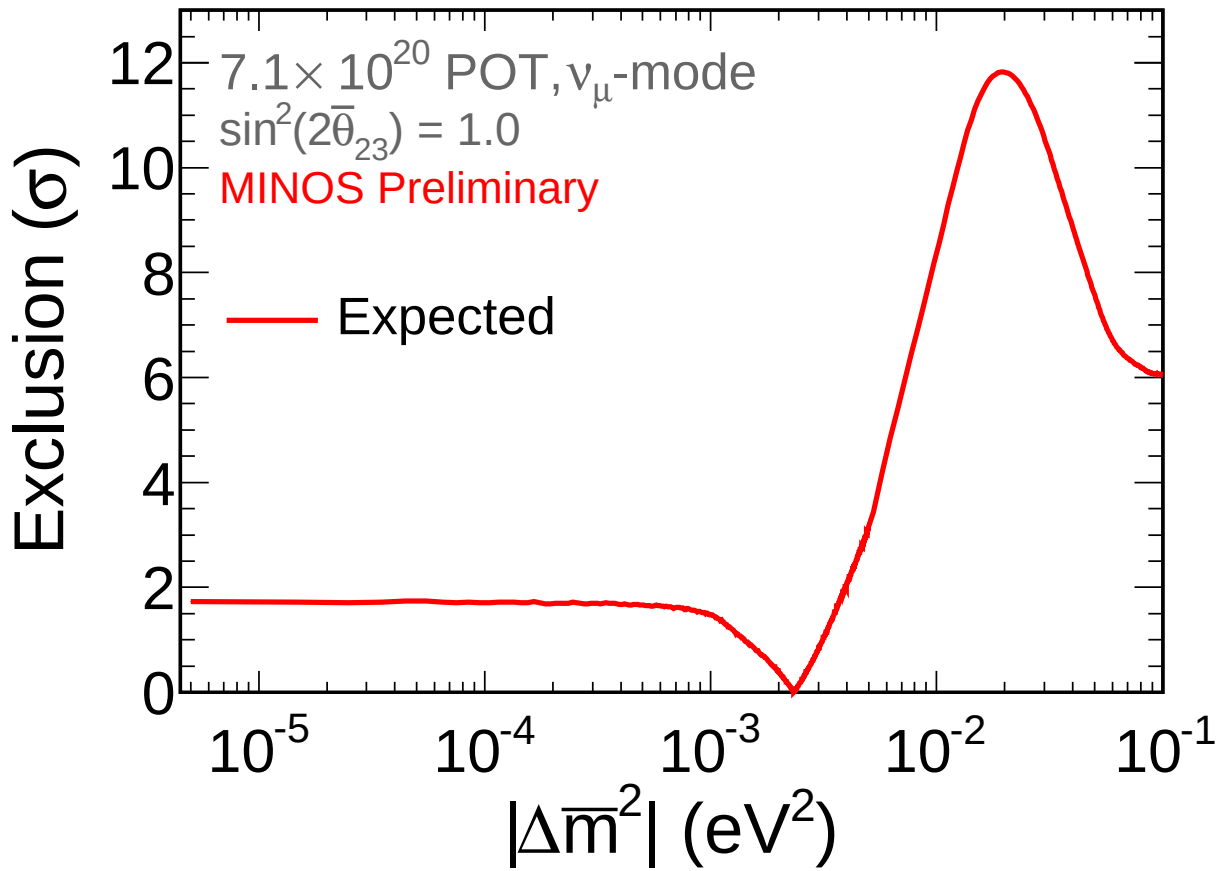

Figure 48: Expected sensitivity of a one-dimensional fit of $\Delta\bar{m}^2$ at maximal mixing, showing the values excluded by this result. The sensitivity is determined by extrapolating Near Detector Monte Carlo simulations and fitting them with Far Detector Monte Carlo simulations oscillated at $|\Delta\bar{m}^2_{atm}| = 2.32 \times 10^{-3}$ eV^2 and $\sin^2(2\bar{\theta}_{23}) = 1.0$. At maximal mixing, we expect to exclude $\Delta\bar{m}^2 > 4.92 \times 10^{-3}$ eV^2 at a 3 σ significance.

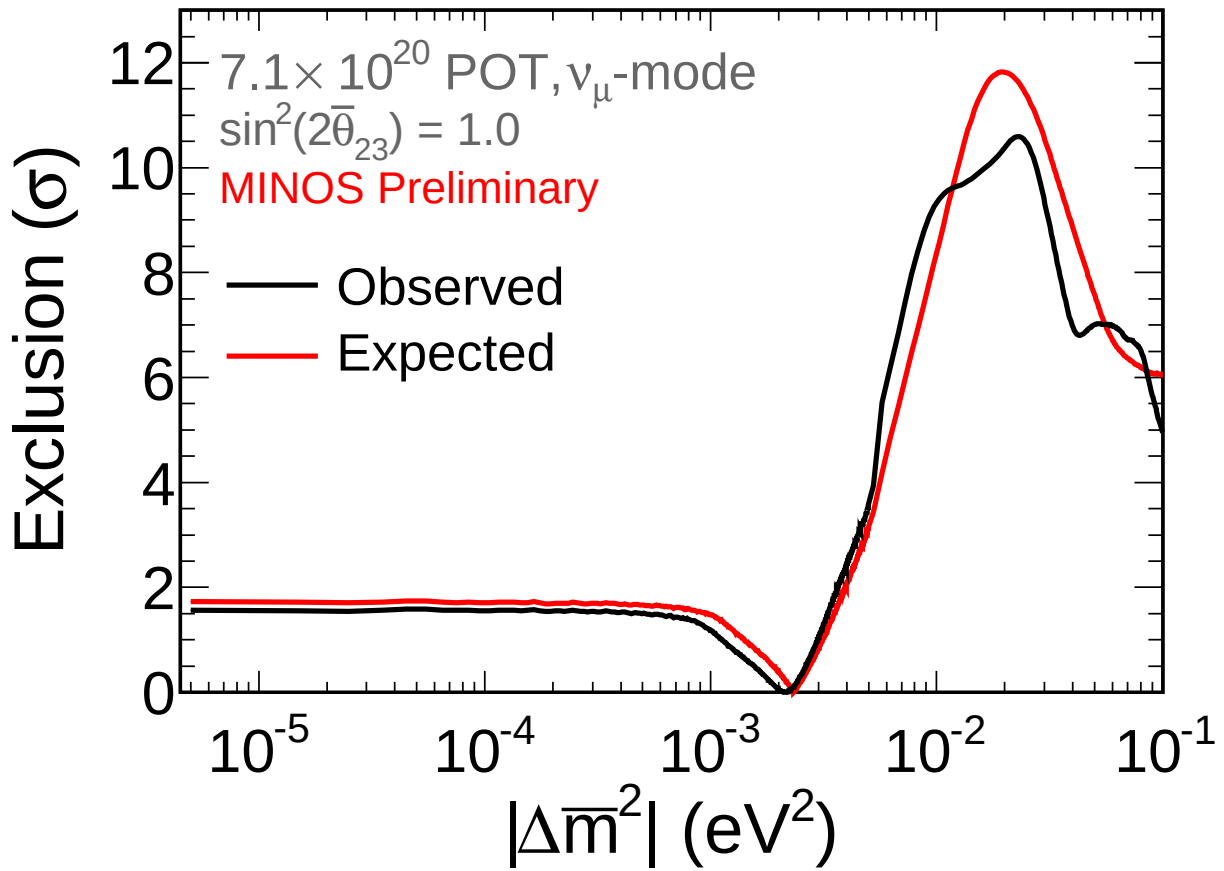

Figure 49: One-dimensional fit of $\Delta\bar{m}^2$ at maximal mixing, showing the values excluded by this result (black line), overlaid with the expected sensitivity of the fit (red line). The sensitivity is determined by extrapolating Near Detector Monte Carlo simulations and fitting them with Far Detector Monte Carlo simulations oscillated at $|\Delta\bar{m}^2_{atm}| = 2.32\times10^{-3}$ eV^2 and $\sin^2(2\bar{\theta}_{23}) = 1.0$. At maximal mixing, we exclude $\Delta\bar{m}^2 > 4.49 \times 10^{-3}$ eV^2 at a 3 σ significance.

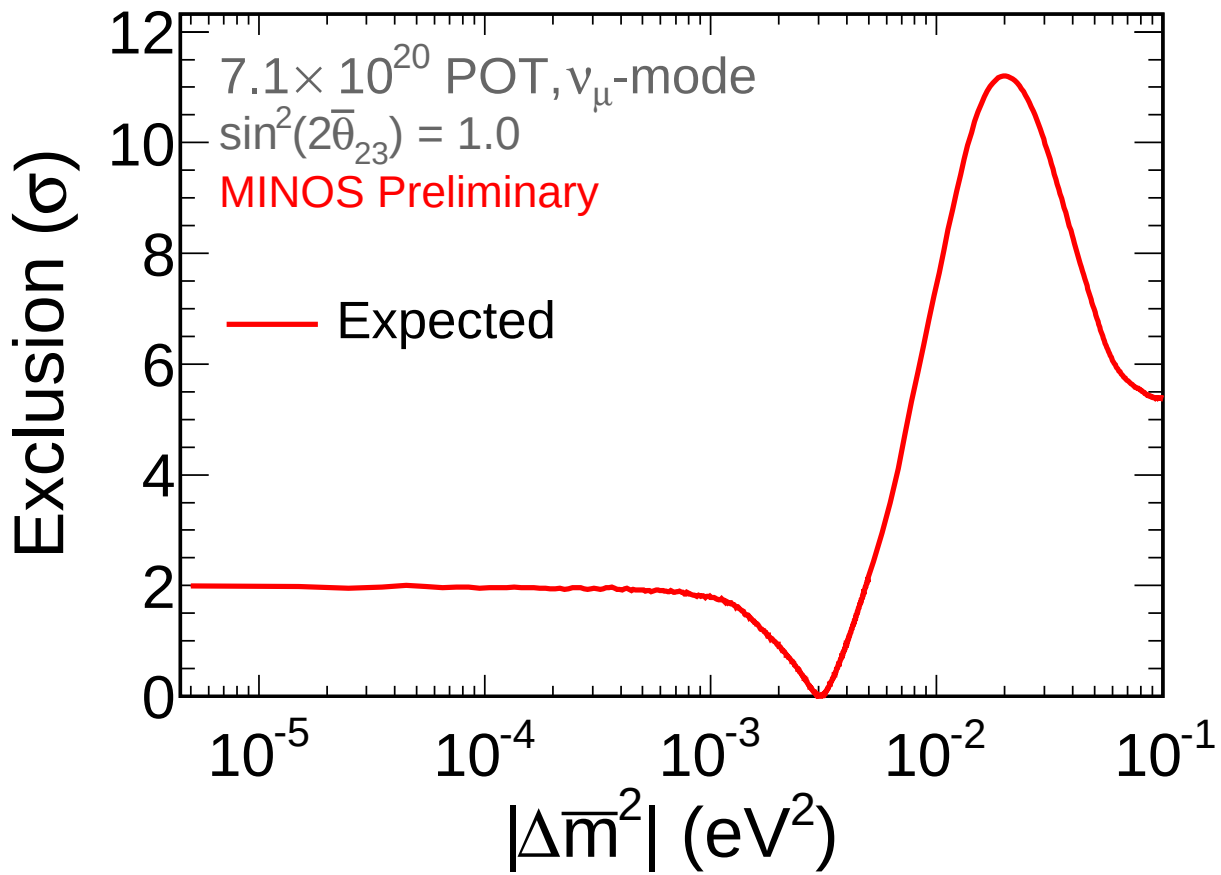

Figure 50: Expected sensitivity of a one-dimensional fit of $\Delta\bar{m}^2$ at maximal mixing, showing the values excluded by this result. The sensitivity is determined by extrapolating Near Detector Monte Carlo simulations and fitting them with Far Detector Monte Carlo simulations oscillated at $|\Delta\bar{m}^2_{atm}| = 3.36 \times 10^{-3}$ eV^2 and $\sin^2(2\bar{\theta}_{23}) = 0.86$. At maximal mixing, we expect to exclude $\Delta\bar{m}^2 > 4.5$ eV^2 at a 3 σ significance.

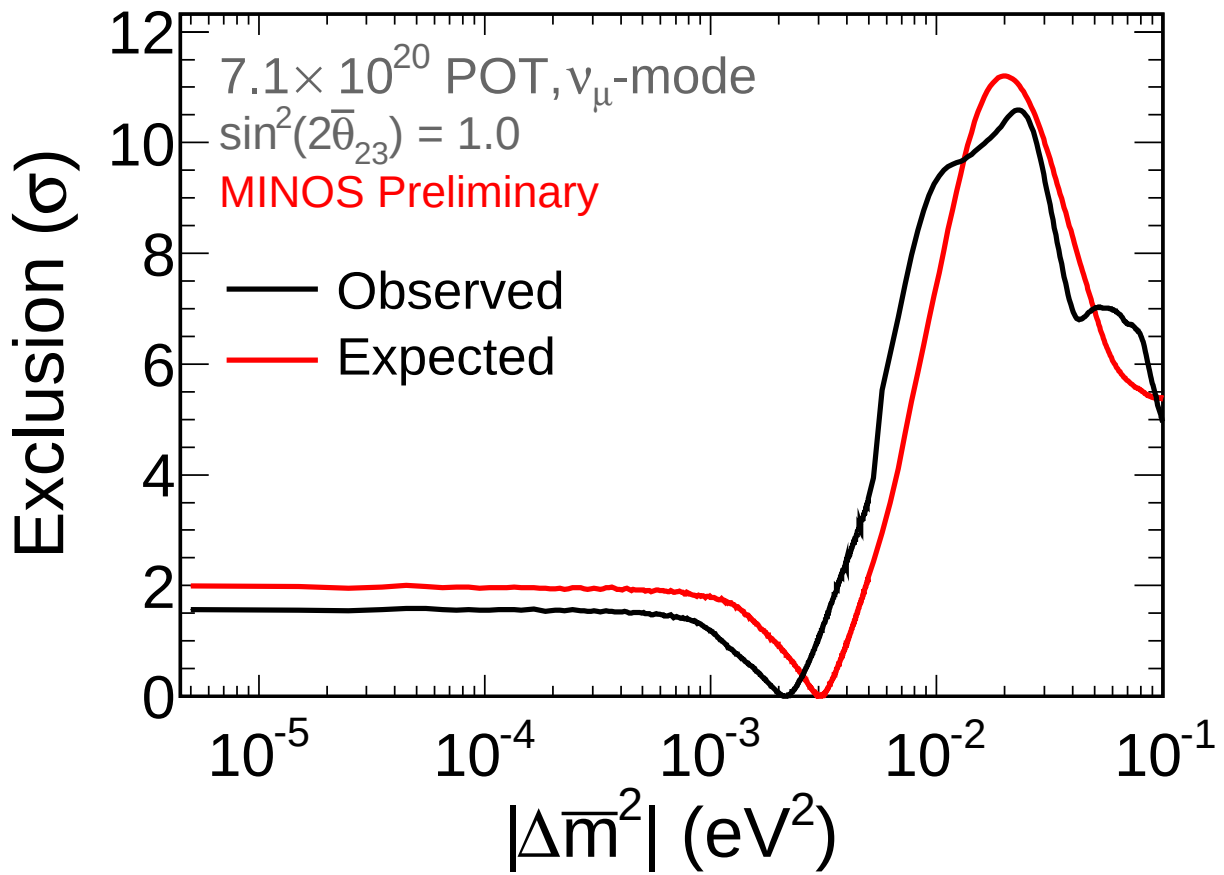

Figure 51: One-dimensional fit of $\Delta\bar{m}^2$ at maximal mixing, showing the values excluded by this result (black line), overlaid with the expected sensitivity of the fit (red line). The sensitivity is determined by extrapolating Near Detector Monte Carlo simulations and fitting them with Far Detector Monte Carlo simulations oscillated at $|\Delta\bar{m}^2_{atm}| = 3.36\times10^{-3}$ eV^2 and $\sin^2(2\bar{\theta}_{23}) = 0.86$. At maximal mixing, we exclude $\Delta\bar{m}^2 > 3.50$ eV^2 at a 3 σ significance.

The power of this data set it to rule out values of $\Delta\overline{m}^2$ corresponding to the region near the peak of the energy spectrum (8 GeV corresponds to 13×10^{-3} eV^2). The sensitivity to atmospheric scale oscillations with this data set is not very strong. Consequently, the best fit point is not very meaningful since there is no closed contour at 90% and the likelihood surface is very flat over a huge range of $\Delta\overline{m}^2$ and $\sin^2(2\overline{\theta}_{23})$. Nevertheless, for information, the best fit point is:

- $\Delta\overline{m}^2 = 18 \times 10^{-3}\ \mathrm{eV}^2, \sin^2(2\overline{\theta}_{23}) = 0.25$

———————————-

What this data says about points of interest:

- Null-oscillations is excluded at 77.4% C.L.
- The neutrino best fit is well within the 1 sigma contour: excluded at just 14.1% C.L. (i.e. not at all!)
- The antineutrino best fit (RHC data) is just within the 1 sigma contour: excluded at 65.2% C.L.

Run Period	Observed Data	7.1e20 MC Oscillated				7.1e20 MC Unoscillated			
		Total	NC	WS	Tau	Total	NC	WS	Tau
Total	130	136.4	1.2	1.8	0.2	150.3	1.2	2.5	0.0
Runs1+2	43	60.2	0.6	0.8	0.1	66.4	0.6	1.2	0.0
Run3	87	76.2	0.6	0.9	0.1	83.9	0.6	1.3	0.0

Data taken from minos-doc-7872. The oscillated scenario is at the neutrino best fit point.

———————————-

Details of the 1-dimensional FC-corrected fit to $\Delta\overline{m}^2$ **assuming maximal mixing**. Please be very careful never to quote these numbers without the maximal mixing caveat! Note that values of $\Delta\overline{m}^2$ above 1 eV^2 were not considered due to oscillation effects growing to be greater than 1% in the ND above that point.

- Best fit = 2.15×10^{-3} eV^2.
- At 68.3% C.L. we restrict $(1.11 < \Delta\overline{m}^2 < 2.95) \times 10^{-3}$ eV^2.
  Sensitivity is $(1.42 < \Delta\overline{m}^2 < 3.12) \times 10^{-3}$ eV^2.
- At 90% C.L. we **EXCLUDE** $(3.37 < \Delta\overline{m}^2 < 1000) \times 10^{-3}$ eV^2.
  Sensitivity is $\Delta\overline{m}^2 < 0.71 \times 10^{-3}\ \mathrm{eV}^2; 3.57 \times 10^{-3}\ \mathrm{eV}^2 < \Delta\overline{m}^2$.
- At 99.7% C.L. we **EXCLUDE** $(4.49 < \Delta\overline{m}^2 < 1000) \times 10^{-3}$ eV^2.
  Sensitivity is $(4.92 < \Delta\overline{m}^2 < 1000) \times 10^{-3}$ eV^2.

Sensitivity was calculated at the neutrino best fit point.

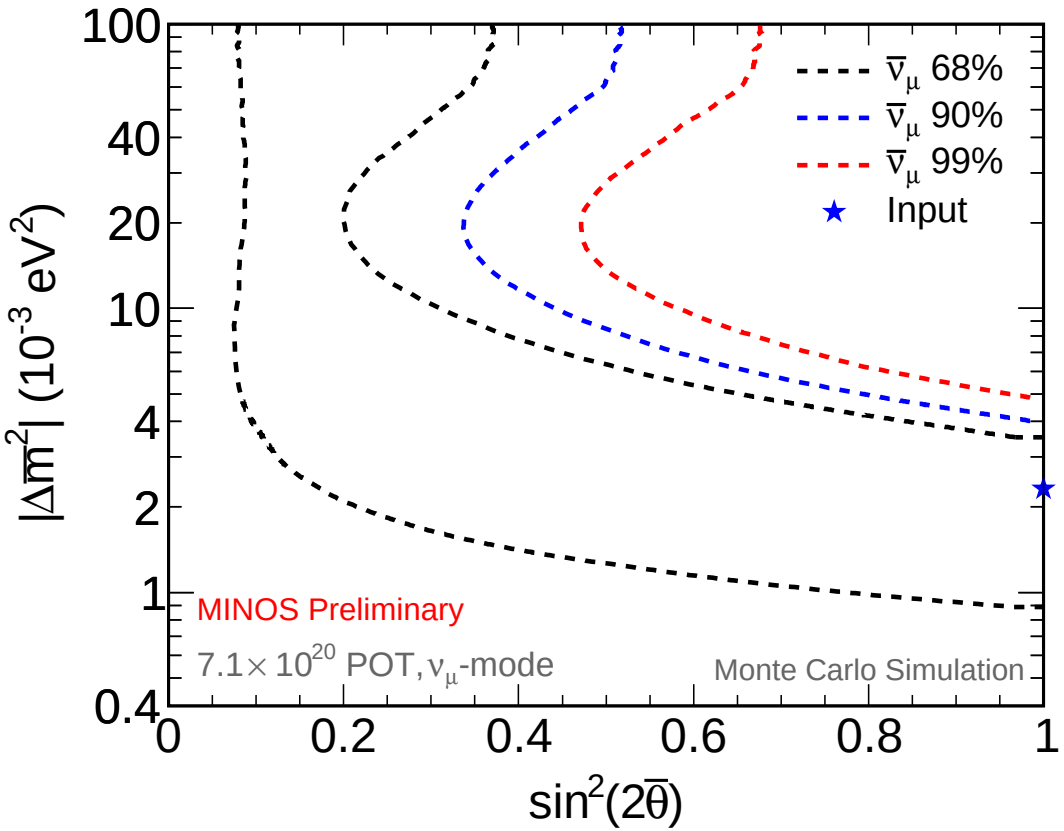

Figure 52: The 68%, 90%, and 99% antineutrino oscillation sensitivity contours as determined from Monte Carlo simulations. The contours are determined using the Feldman-Cousins method, and are obtained by extrapolating Near Detector Monte Carlo simulations and fitting them with Far Detector Monte Carlo simulations oscillated at $|\Delta\bar{m}^2_{atm}| = 2.32 \times 10^{-3}$ eV^2 and $\sin^2(2\bar{\theta}_{23}) = 1.0$.

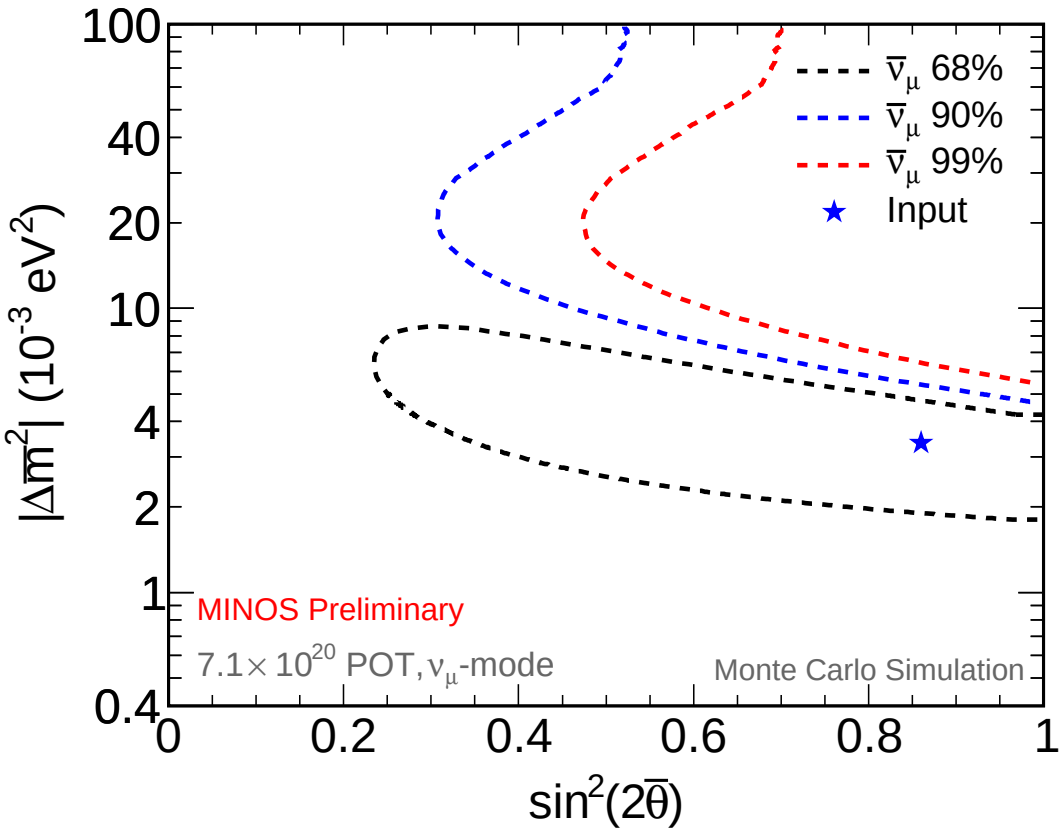

Figure 53: The 68%, 90%, and 99% antineutrino oscillation sensitivity contours as determined from Monte Carlo simulations. The contours are determined using the Feldman-Cousins method, and are obtained by extrapolating Near Detector Monte Carlo simulations and fitting them with Far Detector Monte Carlo simulations oscillated at $|\Delta\bar{m}^2_{atm}| = 3.36 \times 10^{-3}$ eV^2 and $\sin^2(2\bar{\theta}_{23}) = 0.86$.

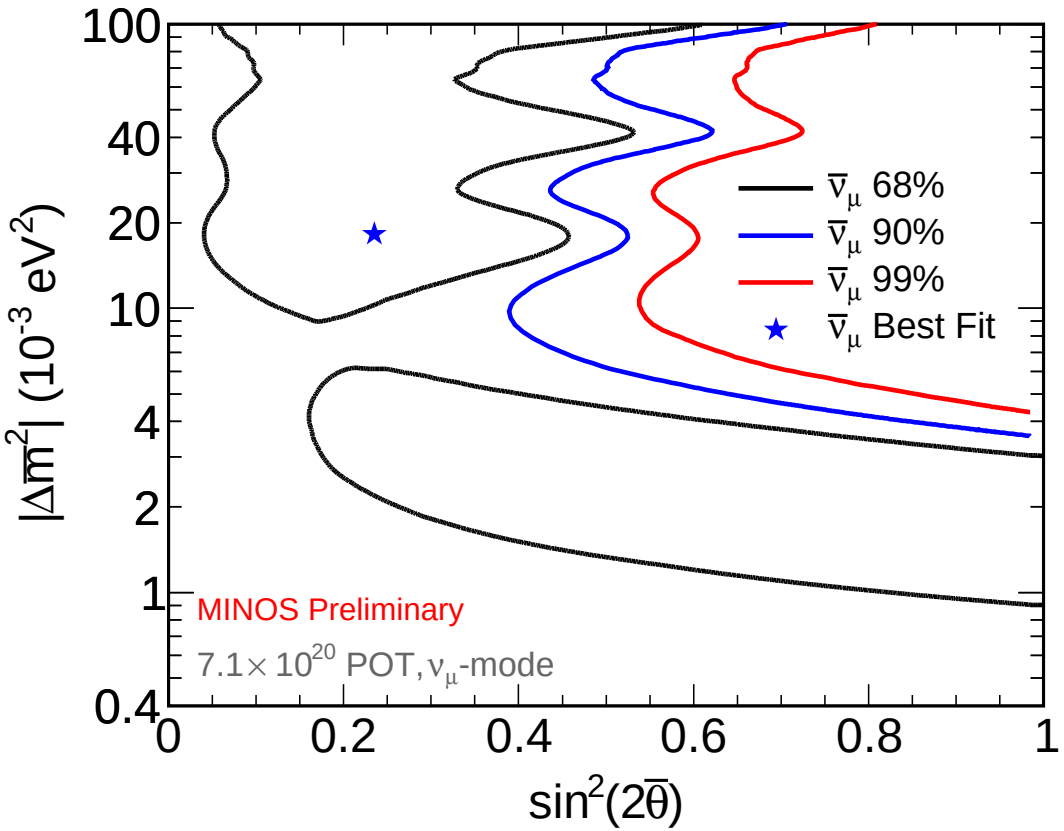

Figure 54: The 68%, 90%, and 99% antineutrino oscillation contours from FHC running. The contours are determined using the Feldman-Cousins method. The best fit is at $|\Delta\bar{m}^2_{atm}| = 18 \times 10^{-3}$ eV^2 and $\sin^2(2\bar{\theta}_{23}) = 0.25$.

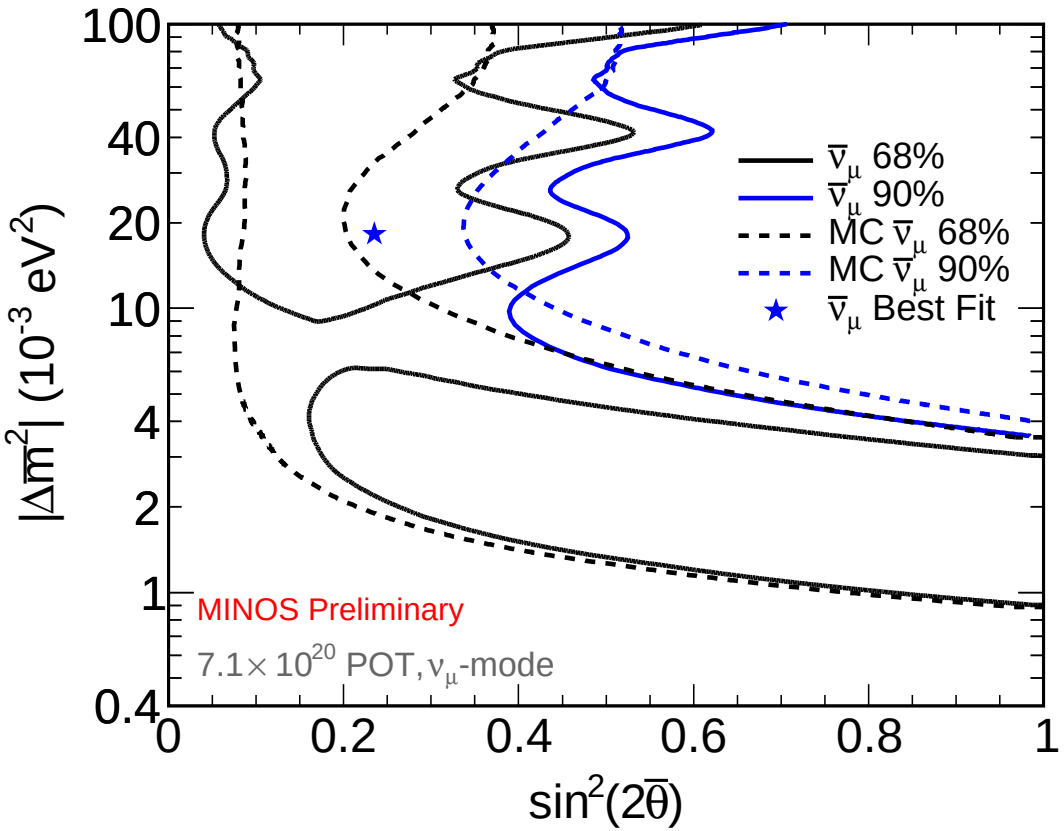

Figure 55: The 68% and 90% antineutrino oscillation sensitivity contours as determined from Monte Carlo simulations overlaid with contours as determined from the FHC running. The sensitivity contours are determined using the Feldman-Cousins method, and are obtained by extrapolating Near Detector Monte Carlo simulations and fitting them with Far Detector Monte Carlo simulations oscillated at $|\Delta\bar{m}^2_{atm}| = 2.32 \times 10^{-3}$ eV^2 and $\sin^2(2\bar{\theta}_{23}) = 1.0$. The best fit is at $|\Delta\bar{m}^2_{atm}| = 18 \times 10^{-3}$ eV^2 and $\sin^2(2\bar{\theta}_{23}) = 0.25$.

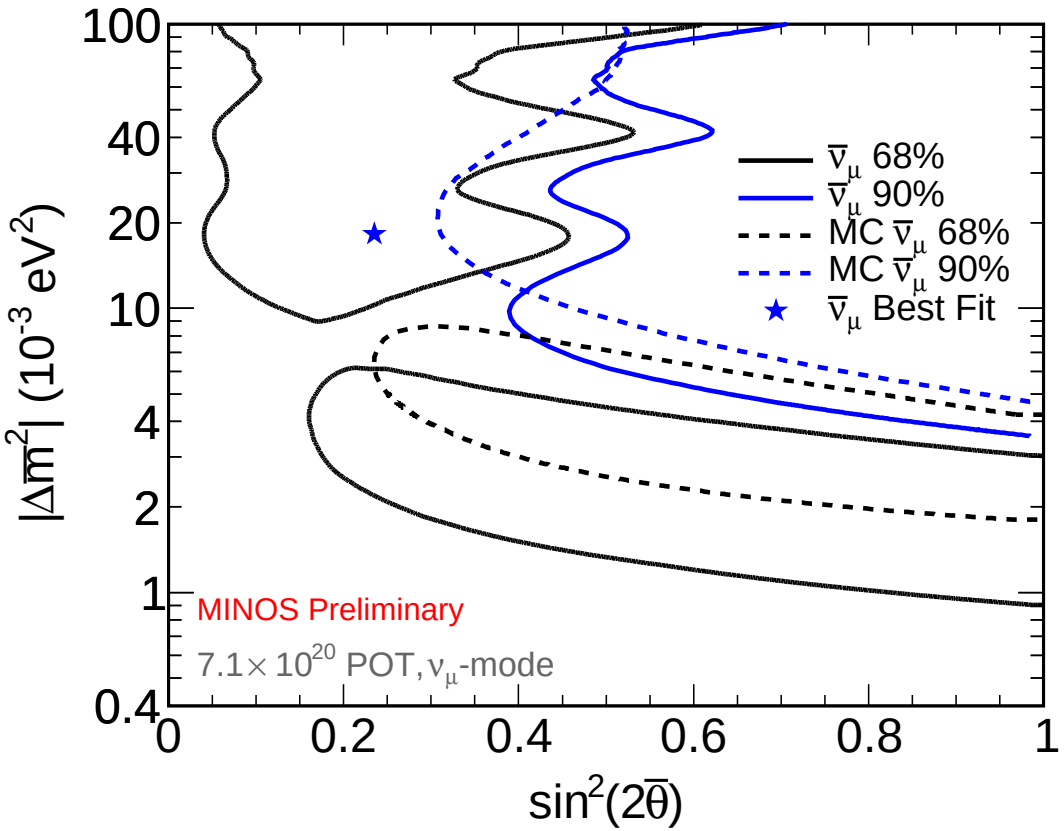

Figure 56: The 68% and 90% antineutrino oscillation sensitivity contours as determined from Monte Carlo simulations overlaid with contours as determined from the FHC running. The sensitivity contours are determined using the Feldman-Cousins method, and are obtained by extrapolating Near Detector Monte Carlo simulations and fitting them with Far Detector Monte Carlo simulations oscillated at $|\Delta\bar{m}^2_{atm}| = 3.36 \times 10^{-3}$ eV^2 and $\sin^2(2\bar{\theta}_{23}) = 0.86$. The best fit is at $|\Delta\bar{m}^2_{atm}| = 18 \times 10^{-3}$ eV^2 and $\sin^2(2\bar{\theta}_{23}) = 0.25$.

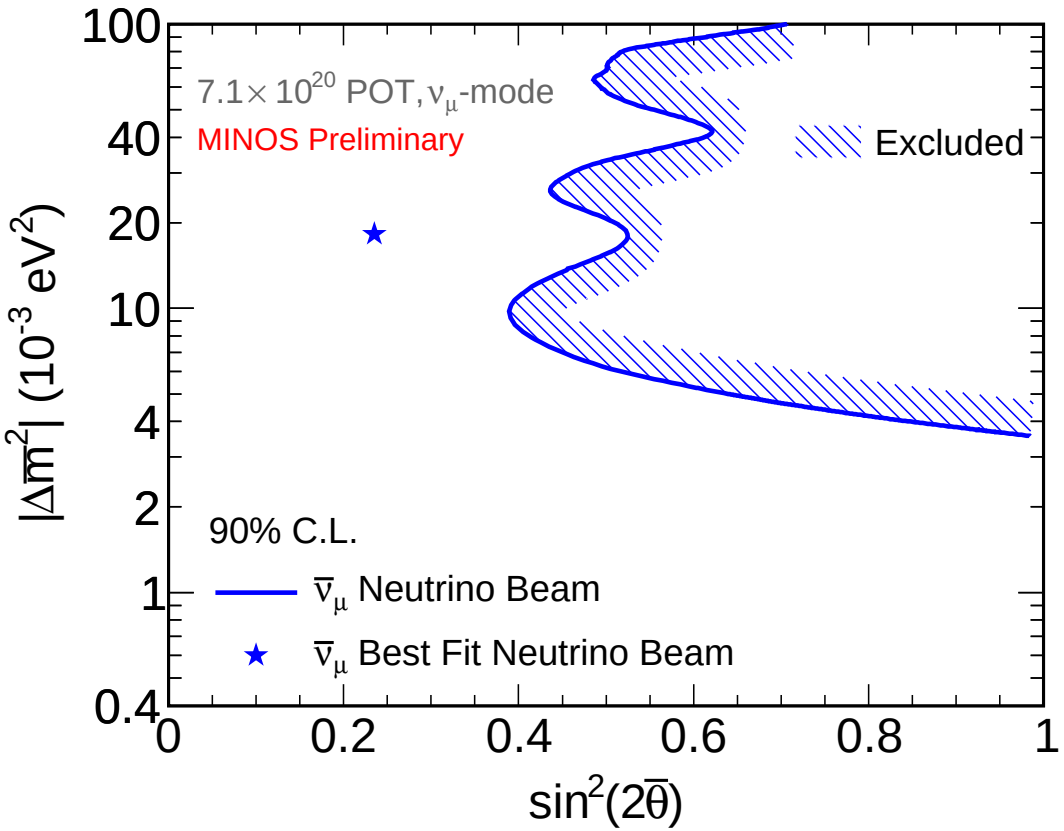

Figure 57: The 90% antineutrino oscillation contour from FHC running. The contour is determined using the Feldman-Cousins method. The best fit is at $|\Delta\bar{m}^2_{atm}| = 18 \times 10^{-3}$ eV^2 and $\sin^2(2\bar{\theta}_{23}) = 0.25$. The hatched area indicates the excluded region.

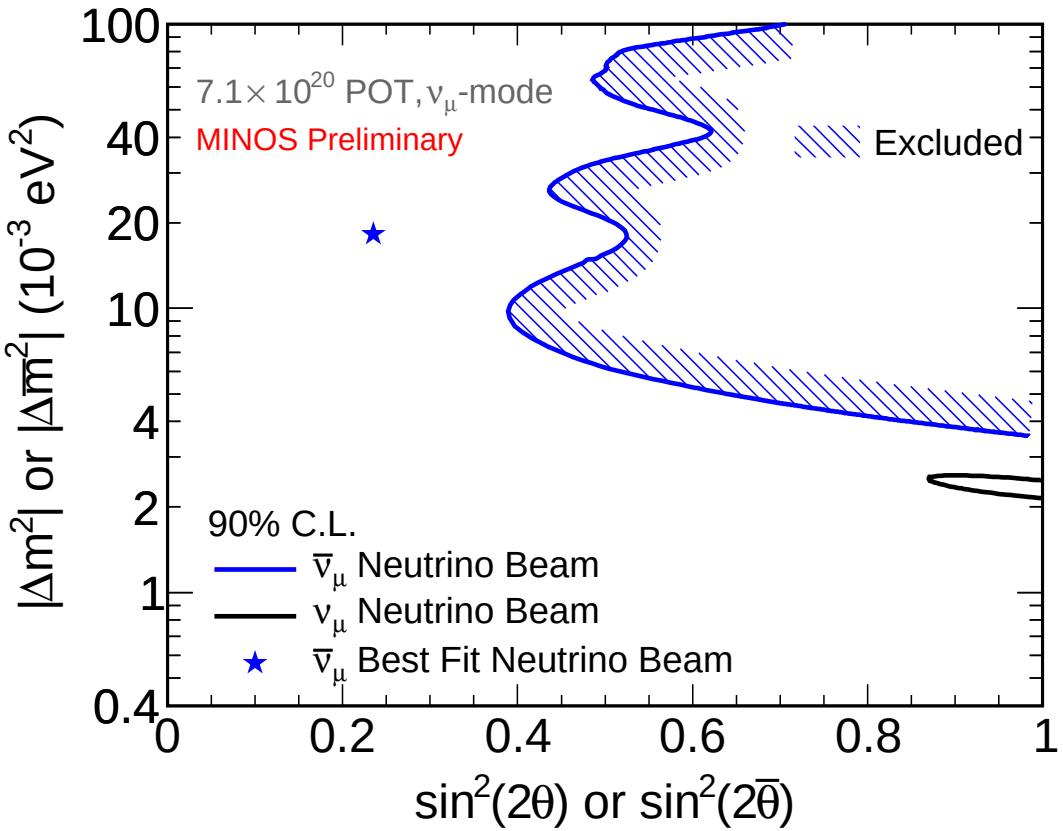

Figure 58: The 90% antineutrino oscillation contours from FHC running, overlaid with the 2010 CC ν_μ result. The contours are determined using the Feldman-Cousins method. The best fit is at $|\Delta\bar{m}^2_{atm}| = 18 \times 10^{-3}$ eV^2 and $\sin^2(2\bar{\theta}_{23}) = 0.25$. The hatched area indicates the excluded region.

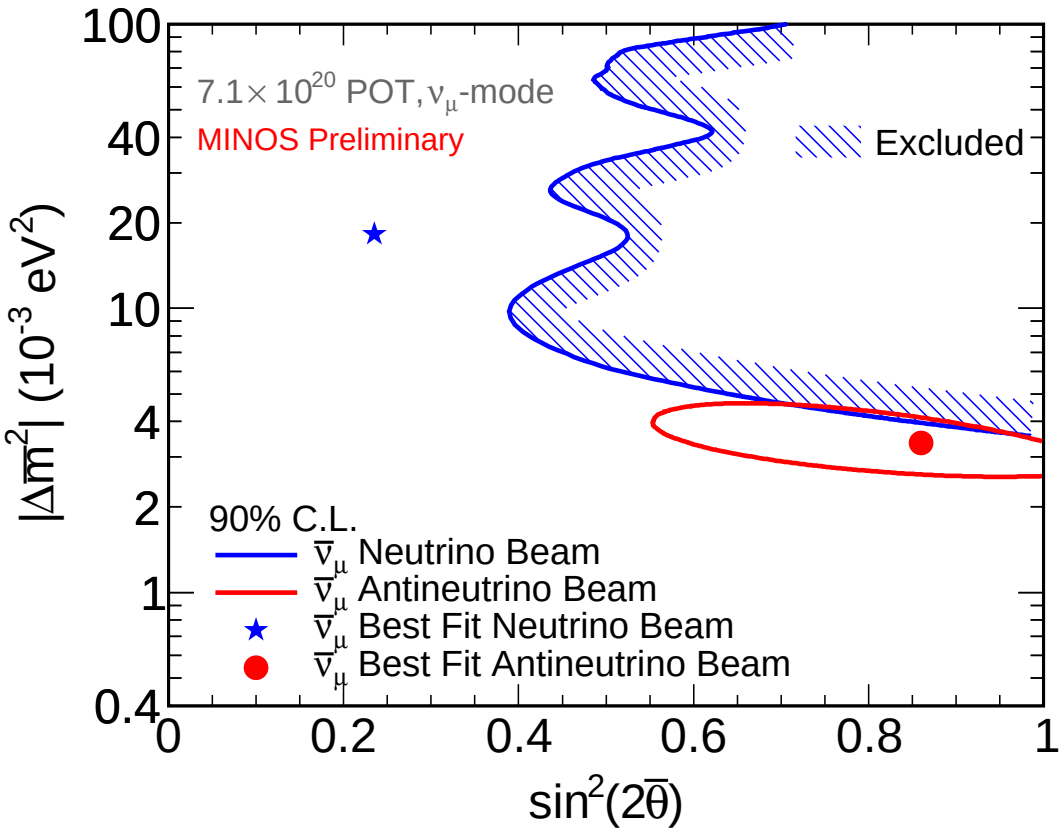

Figure 59: The 90% antineutrino oscillation contours from FHC running, overlaid with the 2010 RHC $\bar{\nu}_\mu$ result. The contours are determined using the Feldman-Cousins method. The best fit is at $|\Delta\bar{m}^2_{atm}| = 18 \times 10^{-3}$ eV^2 and $\sin^2(2\bar{\theta}_{23}) = 0.25$. The hatched area indicates the excluded region.

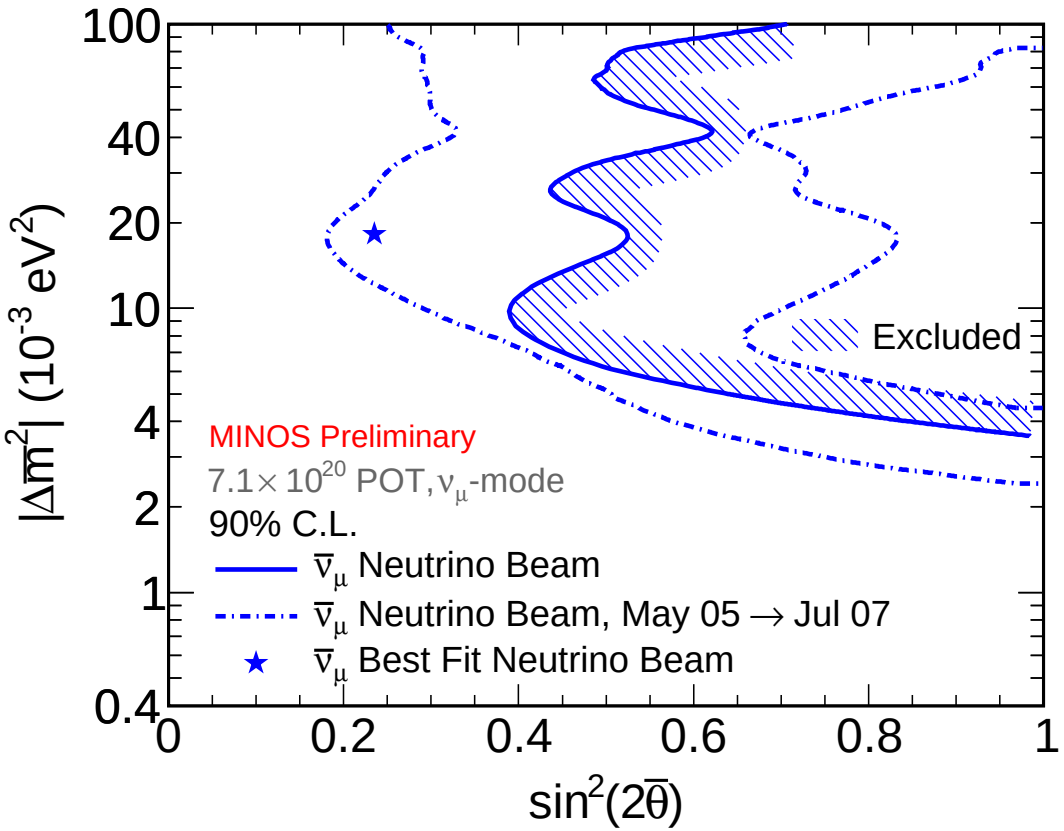

Figure 60: The 90% antineutrino oscillation contours from FHC running, overlaid with the 3.2×10^{20} POT FHC antineutrino result. The contours are determined using the Feldman-Cousins method. The best fit is at $|\Delta\bar{m}^2_{atm}| = 18\times10^{-3}$ eV^2 and $\sin^2(2\bar{\theta}_{23}) = 0.25$. The hatched area indicates the excluded region.

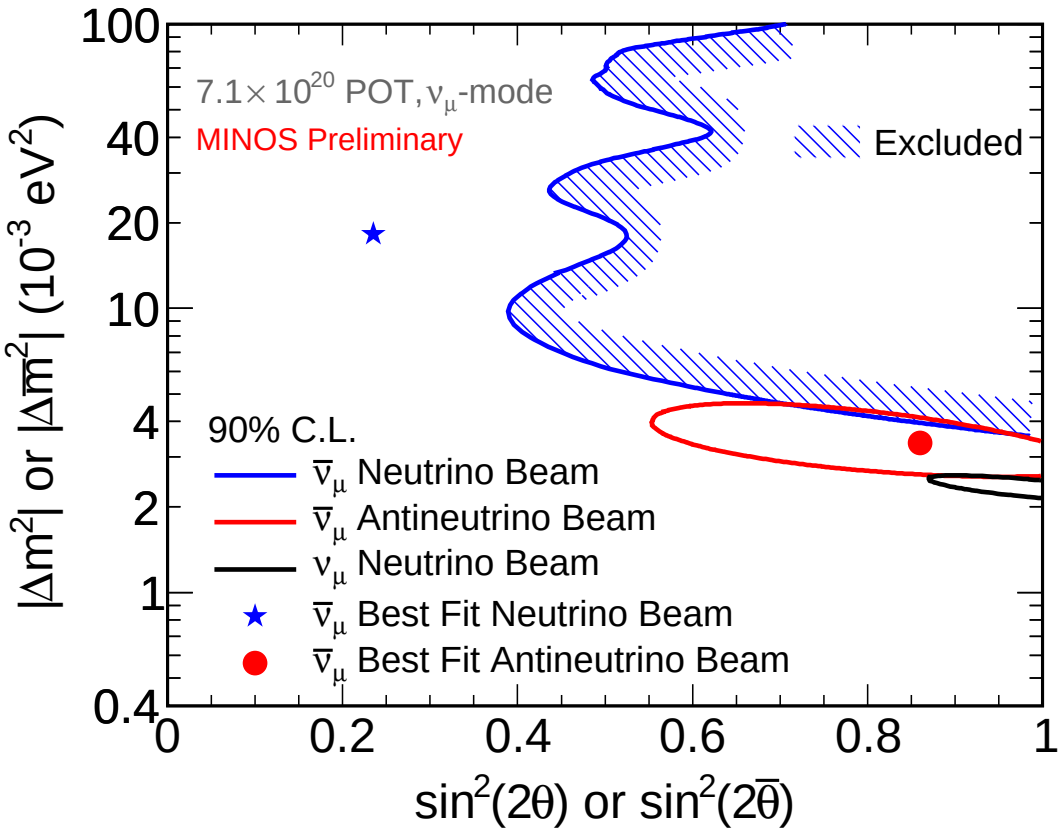

Figure 61: The 90% antineutrino oscillation contours from FHC running, overlaid with the 2010 CC ν_μ result and the 2010 RHC $\bar{\nu}_\mu$ result. The contours are determined using the Feldman-Cousins method. The best fit is at $|\Delta\bar{m}^2_{atm}| = 18 \times 10^{-3}$ eV^2 and $\sin^2(2\bar{\theta}_{23}) = 0.25$. The hatched area indicates the excluded region.

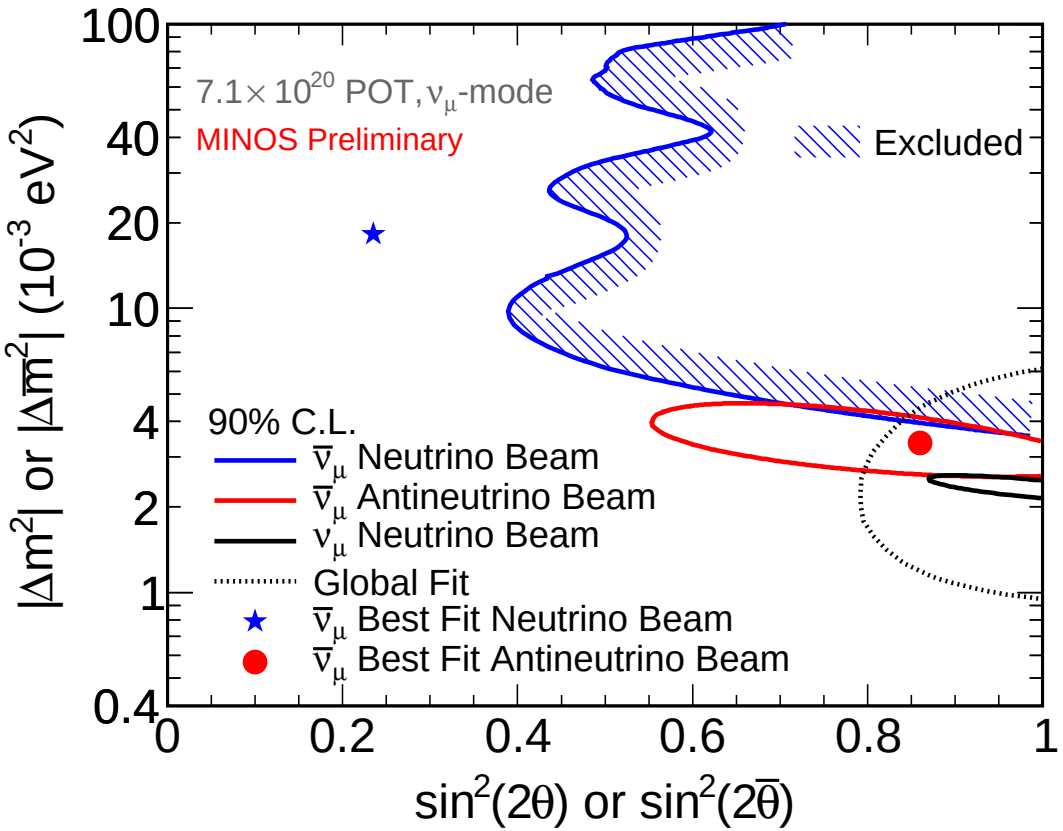

Figure 62: The 90% antineutrino oscillation contours from FHC running, overlaid with the 2010 CC ν_μ result and the 2010 RHC $\bar{\nu}_\mu$ result. The contours are determined using the Feldman-Cousins method. The best fit is at $|\Delta\bar{m}^2_{atm}| = 18 \times 10^{-3}$ eV^2 and $\sin^2(2\bar{\theta}_{23}) = 0.25$. The hatched area indicates the excluded region. They are compared with the 90% confidence global fit without MINOS data from M.C. Gonzalez-Garcia and M. Maltoni (Phys. Rept. 460, 2008). minos-doc-7246